THESIS FOR THE DEGREE OF LICENTIATE OF PHILOSOPHY

Extrasolar Kuiper and asteroid belts
Modelling far-infrared dust emission

JOACHIM WIEGERT

CHALMERS

Department of Earth and Space Sciences
CHALMERS UNIVERSITY OF TECHNOLOGY
Göteborg, Sweden 2014

Extrasolar Kuiper and asteroid belts
Modelling far-infrared dust emission
JOACHIM WIEGERT

Department of Earth and Space Sciences
Chalmers University of Technology
SE–412 96 Göteborg, Sweden
Phone: +46 (0)31–772 1000

Contact information:
Joachim Wiegert
Onsala Space Observatory
Chalmers University of Technology
SE–439 92 Onsala, Sweden

Phone: +46 (0)31–772 5542
E-mail: joachim.wiegert@chalmers.se

Cover image:
Composite of four images showing the Herschel Space Observatory (bottom left) and Spitzer Space Telescope (bottom right) together with particle simulation results of circumstellar discs around α Centauri and Herschel–PACS observations of α Centauri at 100 μm.
Image credits: ESA/AOES Medialab, NASA/JPL–Caltech, and DUNES: DUst around NEarby Stars.

Printed by Chalmers Reproservice
Chalmers University of Technology
Göteborg, Sweden 2014

Extrasolar Kuiper and asteroid belts Modelling far-infrared dust emission

JOACHIM WIEGERT
Department of Earth and Space Sciences
Chalmers University of Technology

Abstract

The first detections of circumstellar dust emission were announced in the mid 1980s. Direct observations of the edge-on disc of β Pictoris provided evidence that the dust was part of possible planetary systems. About a decade later, in 1995, the first confirmed extrasolar planet around a main sequence star (51 Pegasi b) was announced.

The aims here are to study the dynamics and evolution of planetary systems, in which both dust and planets are connected. The aim is also to put the solar system, with its combination of small and large planets, and rings of planetesimals, into a wider context by comparing it with other systems.

To do this we must map out planetary systems around solar-like stars in the solar neighbourhood, through observations and precise modelling.

The nearest solar-like neighbour is α Centauri. This is a binary star with possibilities for planets. We have been able to set upper limits on circumstellar dust emission for these stars to fractional luminosities of a few 10^{-5}. We have also used the primary star, α Centauri A, as a template to better understand how the far-infrared spectrum of solar-like stars behaves. In particular we look at how the chromospheric temperature inversion in the stellar atmosphere will affect dust emission estimates of other stars. We found with the spectrum of α Cen A, that a lack of detection of a temperature minimum in other stars could in reality account for dust emission with a fractional luminosity of 2×10^{-7}.

We are continuing the work on three additional nearby solar-like stars, where one is a binary star with a giant planet. All of these stars already have confirmed dust emission, but may require additional modelling. This is an ongoing project and the results are pending.

Keywords: Stars: binaries - Stars: circumstellar matter - Infrared: stars - Infrared: planetary systems - Submillimeter: stars

Research contributions

This thesis is based on the work contained in **Papers** I **&** II**:**

I R. Liseau, B. Montesinos, G. Olofsson, G. Bryden, J. P. Marshall, D. Ardila, A. Bayo Aran, W. C. Danchi, C. del Burgo, C. Eiroa, S. Ertel, M. C. W. Fridlund, A. V. Krivov, G. L. Pilbratt, A. Roberge, P. Thébault, J. Wiegert, and G. J. White:
α Centauri A in the far infrared. First measurement of the temperature minimum of a star other than the Sun
Astronomy & Astrophysics, 549, L7 (2013)

II J. Wiegert, R. Liseau, P. Thébault, G. Olofsson, A. Mora, G. Bryden, J. P. Marshall, C. Eiroa, B. Montesinos, D. Ardila, J. C. Augereau, A. Bayo Aran, W. C. Danchi, C. del Burgo, S. Ertel, M. C. W. Fridlund, M. Hajigholi, A. V. Krivov, G. L. Pilbratt, A. Roberge, G. J. White, and S. Wolf:
How dusty is α Centauri? Excess or non-excess over the infrared photospheres of main-sequence stars
Astronomy & Astrophysics, 563, A102 (2014)
arXiv:1401.6896 [astro-ph.SR]

Ongoing research projects are described in Chapters 4 and 5.

Acknowledgements

First of all I would like to thank my supervisor, René Liseau, for giving me the opportunity to pursue this field that just happen to also be part of my greatest interests in astronomy. He is a great astronomer and scientist who gladly explains anything I might have missed or misunderstood. You have taught me a lot these last two and a half years, in more than astronomy and physics.

I would also like to thank the members of the DUNES team, in particular Philippe Thébault who has assisted me greatly and always answers whatever questions I might have. There are too many helpful members for me to be able to mention them all here.

Locally I want to thank Karl Torstensson who has done hard work on *complex fields* while I was occupied with finishing the work on α Centauri. And Alessandro Romeo, and Per Bergman, who are always available when I run into problems.

For assisting me with proof-reading this thesis (and more) I must thank both Tuomas Luntila and Magnus Thomasson, plus my parents Lars and Monica who also helped me with the language. The combined effort of you and René has hopefully resulted in an agreeable thesis.

I also want to thank my colleagues at both the observatory and the department at Chalmers. My fellow PhD-students: Eskil, Fabien, Johan, Judit, Lukas, Mitra, Niko, Niklas, Ole Martin, Sofia, and Taïssa, the postdocs and previous PhD-students: Daniel, Francesco, Per B, Kalle again, and Simon. You all make this a wonderful time. Not to forget the administrations at both places and technical support, who are always working hard to make sure that this department functions, Camilla, Glenn, Katarina K, Katarina N, Marita, Paula, and Roger.

My final thanks are for my family and friends. Lars and Monica again, who are always supportive and understanding. Theresa, Benjamin, Daniel, and of course Cassie, you are a crazy bunch. My friends from the university and before (and Hilbert), you know who you are. And especially Beata, for being with me on this and making it a wonderful journey.

Joachim

Contents

Chapter 1

Introduction

Circumstellar environments are highly dynamical and evolving systems, in particular during the earlier eras when they are dominated by thick gas and dust discs. Later, when the central star enters the main sequence, the evolution continues, albeit slower. At this time the stellar flux increases which clears its surroundings from most of the gas and dust and only planets of difference sizes, and rings of planetesimals, remains.

These rings of planetesimals are important for the circumstellar dust this thesis discusses. Gravitational influences from surrounding planets will create collisions in these rings. Such collisions result in the production of μm sized dust grains, or debris, that spread throughout the planetary disc around the star.

This dust cloud is of course affected by the radiation field from the central star in several ways. One result being that the cloud will be easily heated so that it will exhibit black body-like emission. With sufficient amount of dust being heated this will lead to observable excesses at far-infrared (FIR) wavelengths of the stellar spectrum. The peak wavelengths will depend on the size of the disc and the stellar luminosity.

This dust is however, not long-lived. Continued production of dust is required to sustain a circumstellar dust disc. Thus the presence of dust emission is an indirect indication of the existence of a planetary system around the star. Detailed studies of these dust discs can teach us more on the dynamics of planetary systems and their evolution, and put the solar system into a wider context.

1.1 The famous four

The first circumstellar dust disc outside the solar system was observed already in 1984 at Vega (α Lyrae, spectral class A0 V) by Aumann et al. (1984) with IRAS (Infrared Astronomical Satellite). However, as they saw the dust emission only in the spectral energy distribution (SED) they could not infer any shape. The excess is beyond 12 μm and peaks close to 60 μm. They interpreted this as emission from solid particles at 85 AU from the star, distributed in either a shell or a ring (see Figure 1.1). Since such excess first was observed at Vega, it was also called the "Vega phenomenom".

Just a month later the same year, Smith & Terrile (1984) published their observations of β Pictoris. They announced that they had been able to observe optically a circumstellar disc around the star. They infer that they have detected an edge-on disc of ~ 400 AU in radius (see Figure 1.2). They did not know the age of the star, but inferred that it is probably a young star and they speculated that the disc might be a protoplantery disc in either its younger or older stages. Today we consider β Pictoris to be a young star on the main sequence (spectral class A6 V) with indications that planet formation is still ongoing (see e.g. Zuckerman et al. 2001, Wahhaj et al. 2003, and references therein). Furthermore, Lagrange et al. (2009) were able to directly image a giant planet using the VLT (Very Large Telescope). They infer a mass of $8\,M_{\rm Jup}$ with a semi-major axis of ~ 8 AU.

As more data from IRAS was analysed in the 1980s more indications of circumstellar dust was found. Quite soon Vega-like excesses were found in the spectra of two more stars (see Aumann 1985, Gillett 1986, and references therein, and Figure 1.3), Fomalhaut (α Piscis Australis, spectral class A3 V) and ε Eridani (spectral class K2 V). These four together were sometimes called the "the famous four", as they were the first four stars with confirmed circumstellar dust.

As mentioned, this phenomenon was immediately interpreted as heat emission from $\sim$mm-sized grains, which in turn were interpreted as being either remnants from planet forming discs, or debris (if assumed to lie in a disc). The connection between circumstellar discs, former planetary formation, and the existence of planets is obvious. However, no extrasolar planets (exoplanets) had been confirmed yet at this time.

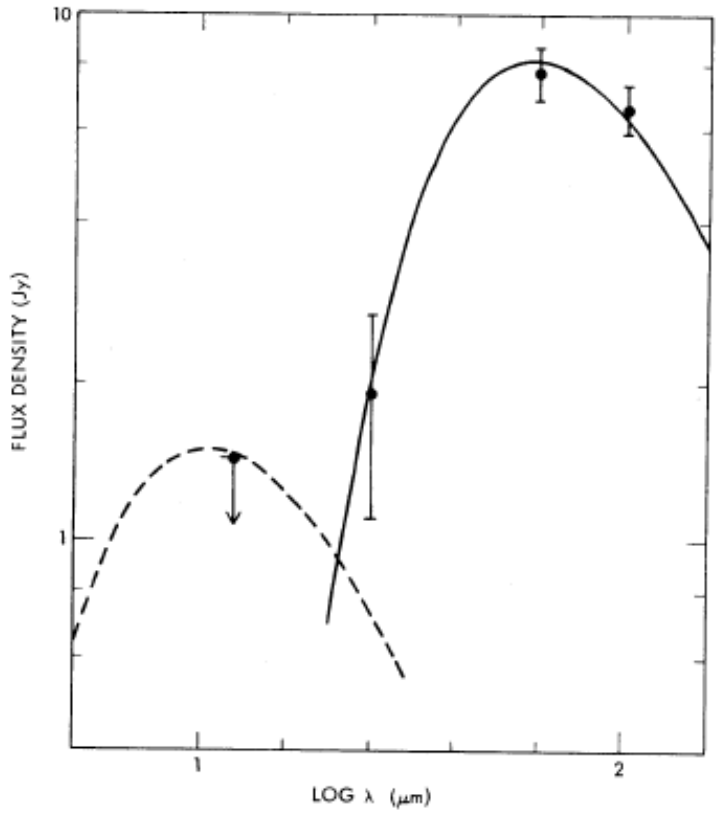

FIG. 1.—Energy distribution of the infrared excess from α Lyr. The error bars represent the 10% calibration uncertainty. The 12 μm upper limit indicates the effect of the 5% uncertainty in the absolute calibration at 12 μm. The solid line represents a 85 K blackbody spectrum with a solid angle of 7×10^{-13} sr fitted to the excess. The dashed line represents a 500 K blackbody spectrum with a solid angle of 6.3×10^{-16} sr arbitrarily fitted to the 12 μm upper limit.

Figure 1.1: Figure 1 from Aumann et al. (1984) with the dust SED from Vega.

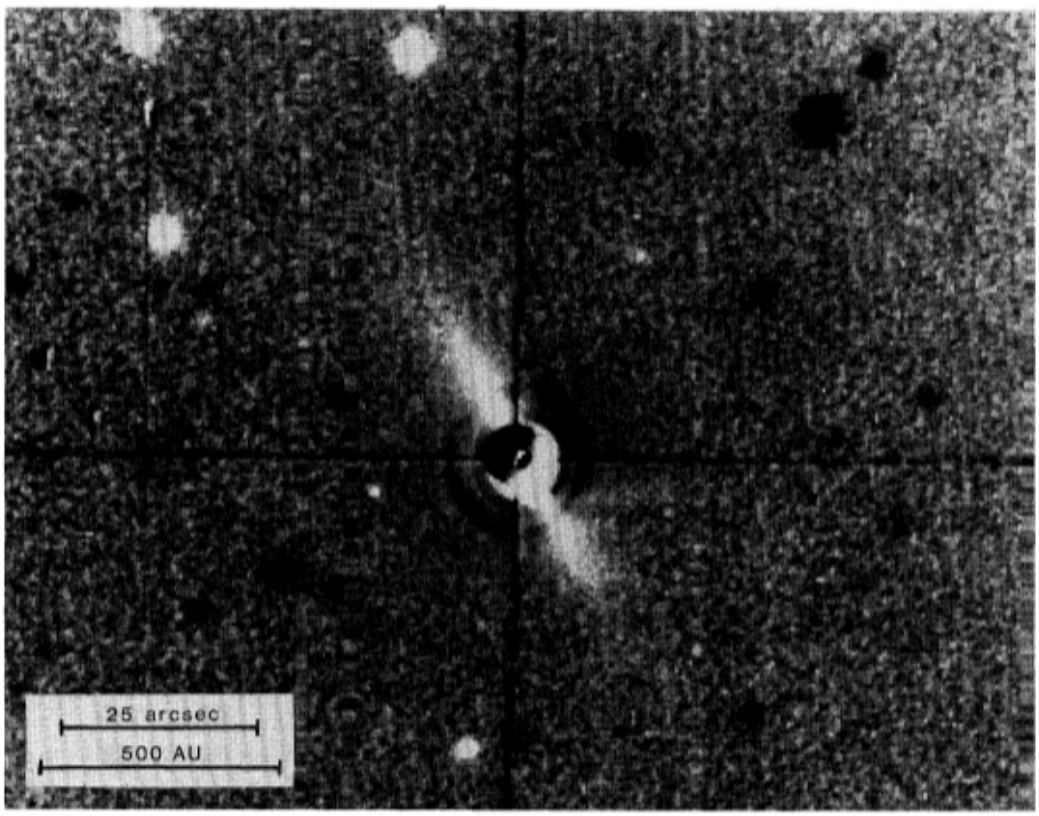

Fig. 1. Ratio image (β Pictoris divided by α Pictoris) showing the edge-on circumstellar disk extending 25 arcsec (400 AU) to the northeast and southwest of the star, which is situated behind an obscuring mask. North is at the top. The dark halo surrounding the mask is caused by imperfect balance in the ratioing process. For further explanation, see text.

Figure 1.2: Figure 1 from Smith & Terrile (1984) with optical observations of the β Pictoris disc.

The connection with planetary systems is through the fact that all of these stars are main sequence stars. Grains of sizes $\lesssim$1 mm are not very long-lived in circumstellar environments due to Poynting–Robertson drag (PR-drag) and radiation pressure. Thus where dust grains exist, there must also exist a sustained dust production which requires belts of planetesimals and planets.

1.2 The first exoplanets

The officially first, confirmed, exoplanet around a main sequence star is 51 Pegasi b, which was first announced by Mayor & Queloz (1995) who were using the radial velocity method. The planet is a gas giant with a mass of $M \sin i \approx 0.5\, M_{\rm Jup}$,

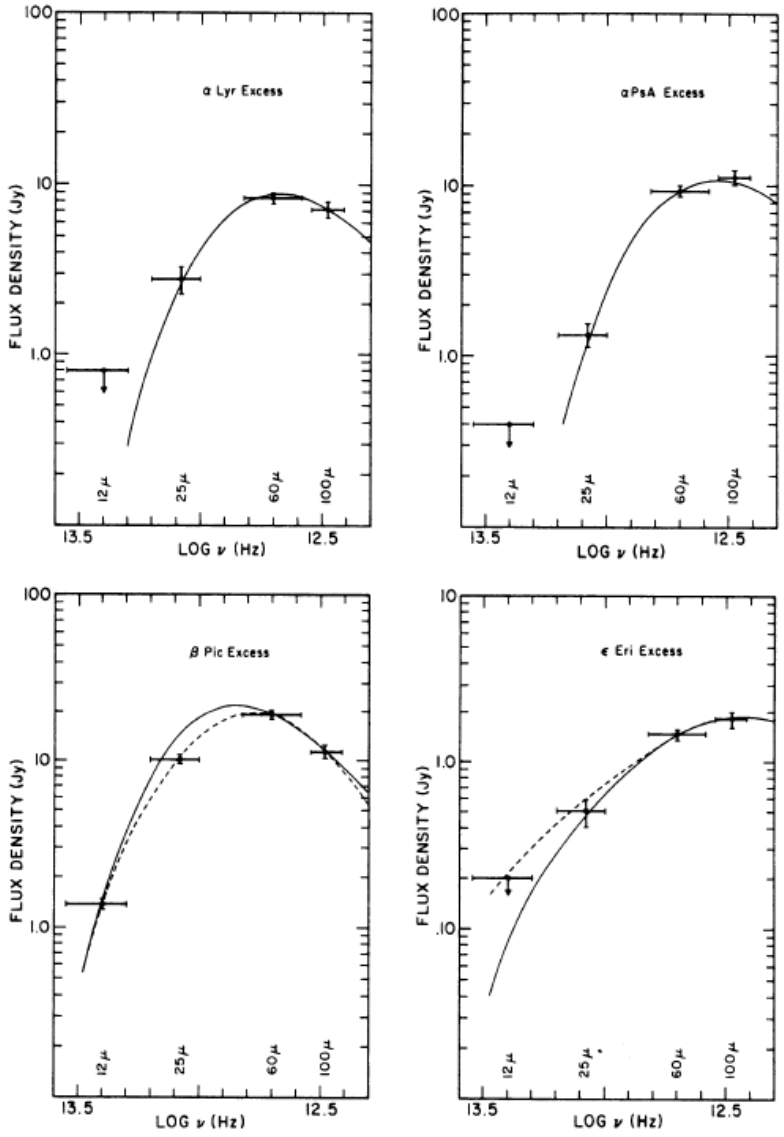

FIGURE 1 - Flux density distributions for the excess emission associated with the program stars. The solid curves for α Lyr, α PsA and ε Eri show fits for the blackbody models described in Table II. The solid curve for β Pic shows fit for blackbody model with γ = 1 and the dashed curve shows fit for the small particle model included in Table I. The dashed curve for ε Eri is for a model with T_{max} = 500K.

Figure 1.3: Figure 1 from Gillett (1986) with the dust SEDs associated with Vega (top left), Fomalhaut (top right), β Pictoris (bottom left), and ε Eridani (bottom right).

and a semi-major axis of 0.05 AU. The star 51 Pegasi (HR 8729, HD 217014, or Gliese 882) is a G5 V star at a 13.7 pc distance. The proximity between the planet and star is why this planet is also considered to be the first *hot Jupiter* found.

However, it is worth noting that already in 1988 a planet was announced around the binary γ Cephei (HR 8974, HIP 116727) by Campbell et al. (1988), also by observing radial velocity. They inferred that they had found a massive planet with $M \sin i \approx 1.6\, M_{\mathrm{Jup}}$ and a period of 2.7 yr. However, Walker et al. (1992) later revoked this discovery, due to uncertainty in the reasons of the found variations. They instead showed that the planetary signal was most probably due to variations in γ Cephei's rotation (they classed the star to be a K0 III star at this time and such variation is common among larger K-stars).

However, Hatzes et al. (2003) later refined the measurements of the velocity variation of the star and found that it does not coincide with the variations first assumed to be due to a planet. The star was also reclassified to a K1 IV star. The most likely explanation is a planet with mass $M \sin i = 1.7 \pm 0.4\, M_{\mathrm{Jup}}$ and a semi-major axis of 2.13 AU, denoted γ Cephei Ab.

As a curiosity, it is also worth mentioning the discoveries by Wolszczan & Frail (1992). They reported finding evidence for two, or more, planet massed objects around the millisecond pulsar PSR1257+12. They proposed the existence of two planets with masses of at least 2.8 and $3.4\, M_{\oplus}$ with semi-major axes of 0.47 and 0.36 AU respectively.

The discoveries by Mayor & Queloz (1995) are nevertheless the first confirmed observations of an exoplanet around a main sequence star. This also marked the birth of a whole new field in astronomy, where now, after almost 20 years, there are 1781 confirmed planets reported in 1100 systems[1]. By combining exoplanet discoveries with circumstellar dust disc findings one can finally start to understand the inner workings of planetary systems and their evolution.

1.3 Dust discs and planets, putting it into context

It is now convenient to take a look back at the solar system, because one of the general goals in this field is to put the solar system into a wider context. An outside observer with technology not much more advanced than ours, would see

[1] As of 2014-03-11, see e.g. `http://exoplanet.eu/`

an extended dust disc with an outer radius of $50-100$ AU, and with a central hole of a radius of 30 AU that is carved out by the four giant planets. The outer dust disc consists of debris produced by the Kuiper belt (also called the Edgeworth–Kuiper belt, EKB, after Kenneth Edgeworth and Gerard Kuiper). The observer might even be able to observe the Zodiacal cloud, an inner debris disc produced by the asteroid belt which stretches inwards from ~ 4 AU radius towards the Sun. Both of these discs would have very weak emission.

The solar system has two planetesimal rings where μm to mm dust/debris particles are produced through collisions and spread through non-gravitational forces to form a disc which is also shaped by the gravitational influences of the planets. Similar dynamics can be expected in other systems and there are already examples of these. In β Pictoris for example, the disc is known to have gaps and rings inside $\lesssim 90$ AU from the star which indicates the presence of giant planets (Wahhaj et al. 2003, and references therein). Lagrange et al. (2009) were able to directly image a gas giant (β Pictoris b) with a mass of $\sim 8\, M_{\rm Jup}$ and semi-major axis of ~ 8 AU.

Another more mysterious case is that of Fomalhaut b. It was first found by Kalas et al. (2008) by direct imaging with the Hubble Space Telescope (HST). Their findings indicate a giant planet at 119 AU from the star. By assuming that this planet is the cause of the inner edge of the dust ring, dynamical modelling indicates that it should have a mass of $\lesssim 3\, \mathrm{M_{Jup}}$.

Fomalhaut b's existence was questioned the next year by Marengo et al. (2009) when they attempted to observe it with *Spitzer* and could not detect it. So the original data was revisited and new observations were done by Currie et al. (2012) who could indeed confirm a substellar object in orbit around Fomalhaut. They suggested a dust enshrouded giant planet of $< 2\, M_{\rm Jup}$ where the Hubble images in fact show scattered light from a dust cloud associated with the planet. Kalas et al. (2013) have since then conducted more observations and studied possible orbits of the candidate planet. They found that Fomalhaut b is on a Keplerian orbit with high eccentricity, and possibly dust belt crossing. This is a highly interesting system to continue observations of.

However, both of these examples are around A-class stars. To find solar system analogues, more observations and detections of dust around FGK-stars are required. A nearby solar-like star would be preferred so that higher resolution

can be achieved.

One of the *Herschel* key-projects is called DUNES, Dust around Nearby Stars[2]. It is dedicated to finding cold dust around nearby solar-like stars (F, G, or K spectral classes), i.e. Kuiper belt analogues.

The obvious example of a nearby solar-like star is the solar neighbour α Centauri. This is a binary with G2 V and K1 V stars (Kervella et al. 2003) at a distance of only 1.3 pc (Söderhjelm 1999) where the primary star is sometimes considered a solar twin.

Simulations have shown that planetary formation is possible here despite its binary nature (see Chapter 3). The higher than normal metallicity of both stars is also in favour of existing planetary systems (Maldonado et al. 2012).

Holman & Wiegert 1999 showed that circumstellar orbits are stable inside ~ 3 AU of each star. A planet has been suggested to exist by Dumusque et al. (2012) around the companion star, α Centauri B, making this the nearest detected exoplanet (previously it was the candidate ε Eridani b, Hatzes et al. 2000). However, this planet is difficult to detect with its Earth-like mass (only $1.3\,M_{\oplus}$, and a semi-major axis of 0.04 AU), and it has yet to be confirmed. Hatzes (2013) for example could not find evidence for it when revisiting the data. Evidently it is possible that there exist planets around these stars (with one possible detection). The question is then how much dust there is and what more we can learn from using α Centauri as a nearby laboratory?

1.3.1 *Herschel* Space Observatory

Herschel is an ESA far-infrared/submillimetre (FIR/submm) space telescope (Pilbratt et al. 2010) with a 3.5 m dish. It was launched by ESA in May 2009 and put into orbit around L2 of the Earth-Sun system (the second Lagrangian point). By the end of April 2013 it ran out of liquid helium, its main coolant, and was decommissioned later that same year.

It was equipped with two photometers, PACS (Photodetecting Array Camera and Spectrometer, Poglitsch et al. 2010) and SPIRE (Spectral and Photometric Imaging Receiver, Griffin et al. 2010, and one heterodyne instrument, HIFI (Heterodyne Instrument for the Far Infrared, de Graauw et al. 2010).

[2]http://www.mpia-hd.mpg.de/DUNES/

The PACS provided photometry at the wavelengths 70, 100, and $160\,\mu$m which was most useful for projects like DUNES. Exo–Kuiper belts can, for example, be expected to have their strongest emission at these wavelengths due to the temperature of dust at Kuiper belt-like distances to a solar-like star. PACS $100\,\mu$m also provided the best sensitivity for searching for EKBs (Eiroa et al. 2013). SPIRE observations at 250, 350, and $500\,\mu$m could then complement the PACS observations to constrain the shape of the Rayleigh-Jeans tail of the dust emission.

1.4 Structure of the thesis

This thesis is structured in the following way: in Chapter 2 I summarise the physics required to correctly model dust discs and their emission. In Chapter 3 I summarise the work done on α Centauri and the results published in Paper I and II, and new results based on simulations with higher resolution. In Chapter 4 I introduce an ongoing project under the working-title of *Complex fields*, and finally the outlook for the future and appended papers are summarised in Chapter 5.

Chapter 2

Physics of circumstellar dust

Planetary systems are highly dynamical and in constant evolution. Everything from the largest bodies such as gas giants to the smallest planetesimals and dust grains are always interacting. In this chapter I summarise the most important physics used for modelling circumstellar discs. These are divided in two parts, dynamics (orbits and motions of dust grains) and radiative transfer.

First of all, one must consider the system we are modelling. Is it a binary star and are there any large or small planets? This sets constrains that a realistic disc must satisfy and can also give indications of the dynamics in the disc, e.g. where we can expect to find the dust producing planetesimal rings. Where we expect to find dust must of course also coincide with what temperatures we can infer to the dust from the observed dust emission. If this agreement can not be met, one must re-think the dust disc model from scratch, maybe even reject the idea that we have observed circumstellar dust.

Grain properties, which are directly dependent on the dust production, gives us all we need to know for understanding how the dust absorbs and emits radiation. This in turn gives us estimates on physical quantities, e.g. the total dust mass. However, this might be the weakest part in the modelling, as the grain properties most often are based on assumptions. These assumptions are however based on previous studies and experiments. There are for example studies where the contents of the Zodiacal cloud are studied directly, there are also experiments on how dust grains collide and fragment, and there exist large scale simulations of collisions and disc dynamics (see e.g. Krivov 2010; Aumatell & Wurm 2011; Moro-Martin 2013). However, there exist almost no direct measurements of the

grain properties of dust of other stars. It is possible in some circumstances to constrain some grain properties (the constituents for example) by looking for certain resonances in the emission. However, most often the wavelength resolution is not high enough and the observed data will mostly follow some approximate black body.

In the final parts of this chapter I try to connect these points in a summary on radiative transfer in the dust disc. But first I summarise the equations used, how they are interconnected, and how one can calculate useful physical quantities from the observations and with the help of all the assumptions.

2.1 Disc dynamics

The circumstellar dust considered in this thesis is purely what we refer to as debris, i.e. dust produced by collisions of planetesimals and larger grains in rings of *parent bodies*. It is not dust that is left from the protoplanetary disc (proplyd) but a product of the continued evolution of planetary systems.

In the solar system for example, we have both the asteroid belt and the Kuiper belt that acts as rings of parent bodies for production of dust. The dust from the asteroid belt either gains or loses angular momentum due to interaction with the radiation field from the Sun and the gravitational field from e.g. Jupiter.

The physics that affect the movement of dust grains are summarised in a simple equation of motion (Krivov 2010, and references therein). This can be written as the acceleration

$$\begin{aligned}\ddot{\boldsymbol{r}}_n = &-\frac{G\,M_\star}{r_n^3}\,(1-\mathcal{B}_n)\,\boldsymbol{r}_n \\ &-\frac{(1+SW)\,\mathcal{B}_n}{c}\,\frac{G\,M_\star}{r_n^2}\,(\dot{r}_n\,\hat{r}+\dot{\boldsymbol{r}}_n) \\ &+\sum_i \frac{G\,m_i}{|\boldsymbol{r}_i-\boldsymbol{r}_n|^3}\,(\boldsymbol{r}_i-\boldsymbol{r}_n)\end{aligned} \tag{2.1}$$

for each dust grain n. $M_\star$ is the mass of the central star, $\boldsymbol{r}_n$ is the grain's position relative to the star, r_n is the radial distance between the star and dust grain, m_i is the mass of any planet in the system, and the rest of the terms are described below.

The equation is divided into three parts. The first line describes the gravitational influences from the central star and how that is reduced by radiation pressure. The second line describes Poynting-Robertson (PR) drag and stellar wind drag. Finally, the third line describes gravitational influences from surrounding planets.

The parameter $\mathcal{B}_n$ is the ratio between radiation pressure and gravitation exhibited on particle n from the central star, and SW is the ratio between stellar-wind drag and PR drag (for the Sun about one third, $\sim 0.2 - 0.3$, Gustafson 1994).

The radiation pressure quite simply counteracts the grain's orbit of the central star. A grain released from a parent body in a circular orbit will be bound into an elliptical orbit if $\mathcal{B}_n \leq 0.5$ (see Figure 2.1). Larger $\mathcal{B}_n$ will result in escape trajectories ($0.5 < \mathcal{B}_n < 1$ gives hyperbolic orbits). The boundary between bound orbits and escape trajectories is somewhat smeared if the parent body has an elliptical orbit. However, all grains with $\mathcal{B}_n < 1$ have some kind of Keplerian trajectory (Krivov 2010). This provides one way of finding a lower bound of the size of the dust grains (a_n), because $\mathcal{B}_n$ depends on a_n through

$$\mathcal{B}_n \equiv \frac{F_{\text{rad}}}{F_{\text{grav}}} = \frac{3}{16\,\pi\,c}\frac{L_\star}{G\,M_\star}\frac{1}{\rho_n a_n} \tag{2.2}$$

where $L_\star$ is the luminosity of the star, ρ_n is the mass density of the grain.

The stellar wind-drag and PR drag term instead counteracts the forward motion of the grains, i.e. as a grain orbits the central star it also moves through the radiation field and stellar wind. This results in loss of angular momentum and thus also a decreasing semi-major axis, or a spiral motion inwards towards the star. This effect is greater on larger grains, because smaller grains are more affected by the radiation pressure.

The combination of these forces gives that one can expect to see smaller grains in the outer part of a disc, and larger grains in the inner parts of the disc (Thébault et al. 2010).

Much work has already been done on studying the dynamics and evolution of dust discs. We see examples of particle based work by e.g. Thébault (2012); Stark & Kuchner (2008). Fluid dynamical models are of course also implemented, see e.g. Krivov et al. (2006); Thébault & Augereau (2007). Extensive work has also been done already on planet-disc interaction and the detectability

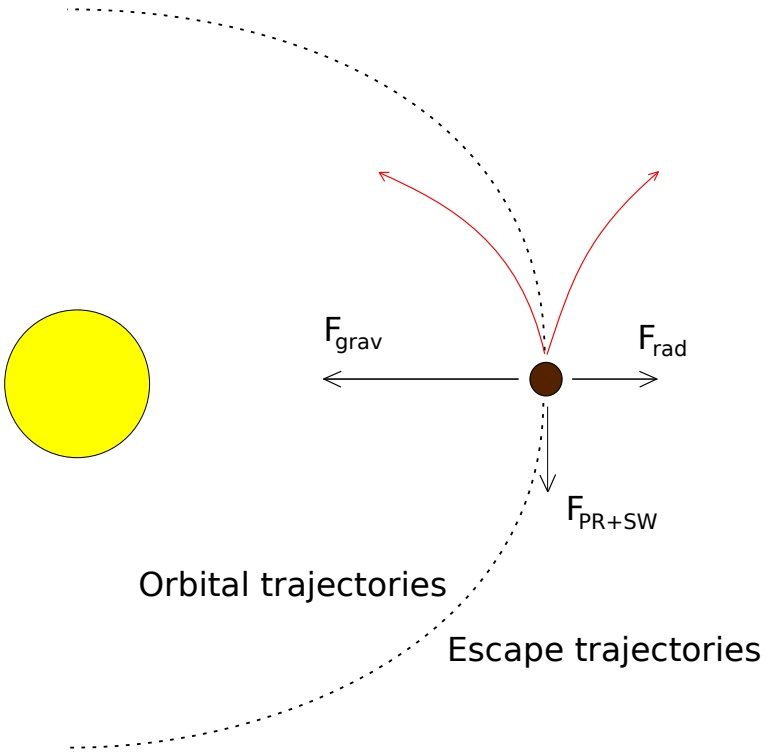

Figure 2.1: Schematic representation of the forces included in Equation 2.1 (except the gravitational influences of planets). Curved red arrows represent possible trajectories of a dust grain released from a parent body in a circular orbit. The area left of the dashed curve (orbital trajectories) is due to $\mathcal{B} \leq 0.5$, and the outer area (escape trajectories) is due to $\mathcal{B} > 0.5$.

of possible gaps (e.g. Regály et al. 2012; Ertel et al. 2012).

However, in some cases it is sufficient to just study the gravitational force's influences on the dust disc, to e.g. find possible disc sizes in binary systems and/or systems with giant planets.

I have written a simple code that solves the motions of N mass-less test particles in a binary system using a Runge-Kutta 4 integrator (more on its usage in Chapter 3). In its current rendition it solves the motions of test particles in arbitary initial positions in a binary system, or a star + giant planet system. It was written to test and confirm previous findings of stable orbits in the α Centauri system.

Future renditions of the same program will be more adaptable. It will allow for an arbitary number of gravitating bodies (stars and planets), at arbitary initial positions, and stable orbits with varying eccentricities.

2.2 Grain properties

A number of grain properties were already seen in Equations 2.1 and 2.2. These properties (and others that follow) are, in contrast with the previously mentioned "global" properties of the discs, microscopic and can sometimes even be studied in laboratories. However, they are essential for the understanding of both the global dynamics of the disc, and the radiative transfer in the disc that will in the end give correct dust emission models.

The first property mentioned before, was the grain size, a_n. As already shown, this affects the orbital dynamics of the grain. However, the range of sizes allowed and the size distribution affect opacity (described later) and the total mass of the dust disc.

The size range is often in the literature limited to be $\lesssim 1\,\mathrm{mm}$ which is useful when comparing results with other studies. This way we effectively exclude any larger grains and any planetesimals.

The lower size limit is often estimated by infering the blow-out radius ($a_{\mathrm{blow-out}}$). The blow-out radius is the smallest radius possible for grains to have stable orbits, i.e. grains that are large enough to not be affected by the combined effects of the radiation field and stellar wind from the central star (Strubbe & Chiang 2006; Plavchan et al. 2009; Krivov 2010). This can be estimated from

$$a_{\mathrm{blow-out}} \approx \frac{3}{8\,\pi\,M_\star\,\rho_{\mathrm{grain}}}\left(\frac{L_\star}{c} + \dot{M}_\star v_{\mathrm{SW}}\right) \tag{2.3}$$

where the first term in the brackets is the radiative momentum rate, and the second term is the mechanical momentum rate. However, the stellar mass loss rate ($\dot{M}_\star$) of $\alpha\,\mathrm{Cen\ A}$ is close to that of the Sun, i.e. $2 \times 10^{-14}\,M_\odot\,\mathrm{yr}^{-1}$, and the average wind speed (v_{SW}) is roughly $\sim 400\,\mathrm{km\,s}^{-1}$ (Wood et al. 2001, 2005). The right term is neglible when compared to the left term, and we can approximate $a_{\mathrm{blow-out}} \approx 0.5 \times \mathcal{B}_n$ (see Equation 2.2).

It has also been shown through simulations (Wyatt et al. 2011; Löhne et al. 2012) that the lower cut-off is smooth. A better approximation of the smallest grains allowed would be around six times the blow-out radius, $a_{\mathrm{min}} \sim 6\,a_{\mathrm{blow-out}}$.

The emission at wavelength λ, however, is dominated by grains of sizes around $\lambda/(2\,\pi)$. This is also the smallest grain size observed at that wavelength.

Grain sizes are most commonly assumed to be distributed as a power law

(Dohnanyi 1969) on the form $n(a_n) \propto a_n^{-q}$ in cases of collisionally dominated discs as the Zodiacal cloud (on a side note similar power-law distributions are assumed for interstellar dust, Mathis et al. 1977). Dohnanyi (1969) found that $q = 3.5$, a number that is most often used in modelling.

Similar power law distributions have been found with the help of simulations in a number of studies since then. More recently by e.g. Bernstein et al. (2004) found $q = 4 \pm 0.5$ for the Kuiper belt, or by Gáspár et al. (2012) who found 3.65. Other recent simulations (e.g. Krivov et al. 2006; Thébault & Augereau 2007; Löhne et al. 2008; Kral et al. 2013; Krivov et al. 2013) find deviations from the power law. However, averages of these variations are still consistent with the steady state of Dohnanyi (1969). Because of this I also generally assume $q = 3.5$ as a "standard" value and also because this is more easily compared with other studies with the same assumption.

A final note on the size distribution (as mentioned earlier) is that the grain sizes tend to be inhomogeneously distributed throughout the disc. Smaller grains tend to be more abundant in the outer parts of the disc and they may even temporarily recide in dynamically unstable regions. This is due collisions and the radiation pressure (see e.g. Thébault et al. 2010). However, so far I have mainly studied grains large enough not to be heavily affected by non-gravitational forces and assume homogeneous distribution for simplicity.

Finally, we have ρ, grain mass density. This is important for e.g. the previously described dynamics, the total dust mass, and also in the optical properties. This can vary, but is typically somewhat smaller than Earth's mean mass density ($5.5\,\mathrm{g\,cm^{-3}}$), between 1 to 5 $\mathrm{g\,cm^{-3}}$ (Moro-Martin 2013) depending on their constituents. A mix of graphite and silicate is often assumed, with or without water ice, and sometimes with iron. Mostly we are forced to just assume something based on what is known about Zodiacal cloud and what has been used in other studies, so that the results are at least easier to compare.

One can however, investigate the possibility of icy grains in the disc. This can be done by calculating the radius of the snow-line, inside which any ice will sublimate. Discs that are dynamically limited to smaller radii may be inside the snow-line and thus not harbor any icy grains, which in turn limits realistic choices of dust opacities and albedo.

Artymowicz (1997) states that the snow-line can be defined as the largest

radial distance from a star at which the sublimation time scale is shorter than all other relevant time scales of the system. An upper limit time scale is the age of the system (some 10^9 yr for solar-like stars) whereas a lower limit can be the orbital period of the grains. The sublimation time scale can be written as (Lamy 1974; Grigorieva et al. 2007)

$$t_{\rm sub} = \frac{a_0\,\rho\,\eta}{\Phi} \tag{2.4}$$

where a_0 is the inital grain size before sublimation (e.g. $1\,$mm), and η is the covering factor (fraction of the grain covered with ice). Φ can in turn be written as

$$\Phi = 3.06\times10^{-4}\,\left(\frac{P_{\rm sat}}{1\,{\rm Pa}}\right)\,\left(\mu\,\frac{1\,{\rm K}}{T}\right)^{1/2}\,{\rm g\,cm^{-2}\,s^{-1}} \tag{2.5}$$

where μ is just the atomic weight of water (i.e. 18 u). The saturation pressure of water vapour, $P_{\rm sat}$ is written within two temperature ranges as

$$\begin{cases} P_{\rm sat} &= 3.56\times10^{12}\,\exp\left(-\frac{6141.67\,{\rm K}}{T}\right)\,{\rm Pa};\ \text{when}\,T\geq170\,{\rm K} \\ P_{\rm sat} &= 7.59\times10^{14}\,\exp\left(-\frac{7043.51\,{\rm K}}{T}\right)\,{\rm Pa};\ \text{when}\,T<170\,{\rm K} \end{cases} \tag{2.6}$$

see Equations 2 and 3 in Grigorieva et al. 2007 and corresponding references therein. Note that the unit in Equations 2.5 and 2.6 have here been changed from torr to Pa.

Finally, to estimate what radial distance each temperature corresponds to it is possible to write that (Liseau et al. 2008)

$$T = T_\star\,\left(\frac{R_\star}{2\,r_{\rm grain}}\right)^{1/2}\,\left(\frac{Q_{\rm abs}}{Q_{\rm em}}\right)^{1/4} \tag{2.7}$$

where $T_\star$ is the effective temperature of the central star, $R_\star$ is the stellar radius, $r_{\rm grain}$ is the semi-major axis of an orbiting grain, and $Q_{\rm abs}$ and $Q_{\rm em}$ are the absorption and emission coefficients (see further details on optical properties of grains in the next section). It is possible to approximate by assuming pure black bodies, i.e. that $Q_{\rm abs} = Q_{\rm em}$.

Table 2.1: List of grain properties

Mass density (ρ)	$1 - 5\,\mathrm{g\,cm^{-3}}$ [(a)]
Lower size limit ($a_{\min}$)	$\sim 6\,a_{\mathrm{blow-out}}$, Equation 2.3
Upper size limit ($a_{\max}$)	1 mm
Temperature/radial distance ($T_{\mathrm{dust}}/r_{\mathrm{grain}}$)	Approximated by Equation 2.7
Snow line	Equations 2.4 through 2.6
Evaporation temperature (T_{vap})	$\sim 1500\,\mathrm{K}$ [(a,b)]

[(a)] Moro-Martin (2013); [(b)] Pollack et al. (1994)

2.3 Dust emission

Here we assume that Kirchhoff's law for thermal radiation, i.e. thermal equilibrium is true (what is absorbed is also emitted), spherical grains, and optically thin discs. This can be described with an energy balance equation, $dE_{\mathrm{abs}}/dt = dE_{\mathrm{emit}}/dt$, where the cooling term for dust is

$$S_{\mathrm{dust}}(\nu) = \int\int 4\,\pi\,a^2\,Q_{\mathrm{abs}}(a)\,\frac{\pi\,B_\nu[T(a,\boldsymbol{r})]}{4\,\pi\,D^2}\,n(a,\boldsymbol{r})\,da\,d\boldsymbol{r}^3 \tag{2.8}$$

which also describes the amount of dust emission received at Earth from a distance D. Here we see how several of the dust properties described earlier are used to describe their emission. For example, the grain size a, density ρ, and absorption efficiency $Q_{\mathrm{abs}}(a)$. Dust temperatures are involved in the black body function $B_\nu[T(a,\boldsymbol{r})]$, and the number density is a function of grain size and position $n(a,\boldsymbol{r})$.

The absorption efficiency is a unitless parameter connected to absorption cross-section (C_{abs} [cm^2]) and mass absorption coefficient (κ_{abs} [cm^{2}g^{-1}]) through

$$Q_{\mathrm{abs}} = \frac{4}{3}\,\frac{C_{\mathrm{abs}}}{a^2} = \kappa_{\mathrm{abs}}\,\frac{4a\rho}{3}. \tag{2.9}$$

Furthermore, absorption, extinction, and albedo are all interrelated through

$$\begin{cases} \kappa_{\mathrm{ext}} &= \kappa_{\mathrm{abs}} + \kappa_{\mathrm{scat}} \\ \kappa_{\mathrm{abs}} &= \kappa_{\mathrm{ext}}\,(1-\eta) \\ \kappa_{\mathrm{scat}} &= \kappa_{\mathrm{ext}}\,\eta \end{cases} \tag{2.10}$$

where η is the albedo of the grains and $\kappa_{\rm scat}$ is the corresponding mass scattering coefficient. All of these opacity coefficients are also functions of frequency. Computation of these belongs to a major field where the effects of e.g. grain composition, grain shape ("fluffiness"), and coatings of ices are studied (e.g. resonances and molecular lines in the extinction curves). Several good examples for the interested reader are Draine (1988); Miyake & Nakagawa (1993); Krügel & Siebenmorgen (1994); Draine (2003, 2006).

Such studies give an ample supply of results to use to estimate these coefficients when modelling dust emission. We usually just use results for compact, bare grains (spherical, non-porous). This is because we simply do not know most of these characteristics of exodebris, as it would require in situ experiments, and we are forced to apply simpler assumptions.

However, it is possible to to study interplanetary dust particles (IPD) caught by the Earth (see Moro-Martin 2013, and references therein). These grains often have irregular, porous shapes, contain silicates, and have mass densities around $1 - 3\,\mathrm{g\ cm^{-3}}$. In the outer parts of the solar system the *Voyager* 1 probe detected dust in the Kuiper belt region ($> 30\,\mathrm{AU}$) with a number density of $\sim 2 \times 10^{-8}\,\mathrm{m^{-3}}$. These data are however poorly calibrated, and they say nothing on the shape or contents of the grains except that the smallest grains detected were $\sim 2\,\mu$m size. Worth mentioning is that *New Horizons* is expected to reach Pluto in July 2015 and will spend at least a decade exploring the Kuiper belt.

Regarding approximations, it is possible to infer a total dust mass from simpler emission models by using some drastic, but sometimes useful, approximations. By assuming isothermal dust in a ring around the star, a ring which only contains grains of one constant size we can follow Hildebrand (1983) and rewrite Equation (2.8) to

$$S_{\rm dust}(\nu) \approx \pi\, a^2\, Q_{\rm abs}(a)\, \frac{B_\nu(T)}{D^2} N_{\rm tot} \tag{2.11}$$

where $N_{\rm tot}$ denotes the total number of dust grains in the ring. Jumping over a few simple steps we can summarise that the total disc mass ($M_{\rm dust}$ of an isothermal ring with grains of size a is

$$M_{\rm dust} = \frac{4\,a\,\rho}{3}\, \frac{S_{\rm dust}(\nu)\, D^2}{Q_{\rm abs}\, B_\nu(T)} = \frac{S_{\rm dust}(\nu)\, D^2}{\kappa_{\rm abs}\, B_\nu(T)}. \tag{2.12}$$

Such approximations are of course useful and can be expanded by assuming several rings to fit the models to the observed dust emission. However, it is also possible to apply more advance radiative transfer simulations when more precise disc and dust models are used. In this project we have applied RADMC–3D by Dullemond (2012), which is a Monte-Carlo based 3D radiative transfer program[1]. This program requires inputs of e.g. opacities, disc shape, positions and spectra of stars, and the output can be both SEDs and images.

[1] http://www.ita.uni-heidelberg.de/~dullemond/software/radmc-3d/

Chapter 3

α Centauri

To be able to study dust discs and exoplanetary systems around solar-like stars in detail we of course turn to nearby stars. We have a unique opportunity here with the solar neighbour α Centuari ($\alpha\,\mathrm{Cen}$).

At a distance of only $1.3\,\mathrm{pc}$ (Söderhjelm 1999), $\alpha\,\mathrm{Cen}$ is the nearest neighbouring star. This is a binary system with the primary, $\alpha\,\mathrm{Cen\,A}$ (a G2 V star), and the companion $\alpha\,\mathrm{Cen\,B}$ (a K1 V star) on an 80 yr orbit with a semi-major axis of $\sim 24\,\mathrm{AU}$ (Torres et al. 2010; Pourbaix et al. 2002). Proxima Centauri (a M6 V star) shares a similar proper motion and seems to be bound to $\alpha\,\mathrm{Cen}$ AB, but with a separation of $\sim 15\,000\,\mathrm{AU}$ (2° southwest from the binary). Assuming a circular orbit gives Proxima Cen a period of roughly $1.3\,\mathrm{Myr}$. Together with Proxima Centauri, the $\alpha\,\mathrm{Cen}$ system is a triple star system where Proxima Cen is sometimes called $\alpha\,\mathrm{Cen\,C}$ for this reason. Because Proxima Cen is currently between the Sun and $\alpha\,\mathrm{Cen}$ it is the nearest known neighbour of the Sun.

The binary, $\alpha\,\mathrm{Cen}$, is one of the brightest stars on the night sky and the brightest in the constellation of Centaurus. It is also known as Rigil Kentaurus (or Rigil Kent), as it is supposed to be the "foot of the Centaur". $\alpha\,\mathrm{Cen\,A}$ has the catalogue designations HD 128620 and HIP 71683, and $\alpha\,\mathrm{Cen\,B}$ has HD 128621 and HIP 71681.

The orbit of the stars allows for circumstellar stable orbits to exist inside $3-4\,\mathrm{AU}$ of each star (Holman & Wiegert 1999), and for circumbinary orbits to exist at radii $\gtrsim 75\,\mathrm{AU}$ from their barycenter (Wiegert & Holman 1997). These are the sizes of the three dynamical stable regions.

Are these regions large enough to have allowed planetary formation? We

know that binarity is not necessarily an obstacle for this as more than 12 % of detected exoplanets are in multiple systems (Roell et al. 2012). The stars also have higher metallicities than the Sun (Maldonado et al. 2012) which is an argument for possible exoplanets. Furthermore, simulations have also shown that planetary formation is possible even though it is a binary. Thébault et al. (2009) for example show that planetary formation around $\alpha\,\mathrm{Cen\,B}$ is possible, but only in the inner parts of the stable zone at $\lesssim 0.5 - 0.75$ AU, i.e. at most at the inner edge of the $\alpha\,\mathrm{Cen\,B}$ habitable zone ($0.5 - 0.9$ AU). More optimistic estimates (Paardekooper & Leinhardt 2010; Xie et al. 2010) give a limit at $1 - 1.5$ AU.

Limited circumstellar planetary systems are clearly possible around the $\alpha\,\mathrm{Cen}$ stars. Radial velocity measurements have shown that an upper limit of planetary masses is $2.5\,M_{\mathrm{Jup}}$ inside 4 AU of either star (Endl et al. 2001). More recently Dumusque et al. (2012) presented results from their substantial radial velocity data set from which they suggest an Earth-like planet of $1.13\,M_{\oplus}$ around $\alpha\,\mathrm{Cen\,B}$ with a semi-major axis of 0.04 AU (denoted $\alpha\,\mathrm{Cen\,Bb}$). This is evidently on the limit of what can be measured, because when Hatzes (2013) used these data for his analysis he was not able to find this planet.

Obviously $\alpha\,\mathrm{Cen}$ is an extremely nearby and intersting system with potential for associated planets. With this in mind, we and DUNES used observations from *Herschel*, *Spitzer*, and APEX (the Atacama Pathfinder Experiment) to investigate possible amounts of dust around these stars. The results are presented in Papers I and II, and summarised in this chapter together with more details concerning simulations and modelling.

3.1 Binary dynamics and simulations

Previous work on the dynamics of these stars resulted in an semi-analytical expression that describes the semi-major axis of stable circumstellar orbits around each star (Holman & Wiegert 1999). The largest stable semi-major axis (hereon the critical semi-major axis, r_{crit}) can be written as

$$r_{\mathrm{crit}} = \left(c_1 + c_2\,\mu + c_3\,e + c_4\,\mu\,e + c_5\,e^2 + c_6\,\mu\,e^2\right)\,r_{\mathrm{AB}} \tag{3.1}$$

where $\mu = M_{\mathrm{B}}/(M_{\mathrm{A}} + M_{\mathrm{B}})$, i.e. the fractional mass of the binary companion, e is the binary eccentricity, r_{AB} is the binary semi-major axis, and c_1 through c_6 are

Table 3.1: Properties of the α Centauri binary

	α Cen A	α Cen B
Sp.type[a]	G2 V	K1 V
$T_{\rm eff}$ (K)[b]	5824 ± 24	5223 ± 62
$L_{\rm star}$ ($L_\odot$)[b]	$1.549^{+0.029}_{-0.028}$	$0.498^{+0.025}_{-0.024}$
$M_{\rm star}$ ($M_\odot$)[bc]	1.105 ± 0.007	0.934 ± 0.006
$R_{\rm star}$ ($R_\odot$)[a]	1.224 ± 0.003	0.863 ± 0.005
$r_{\rm crit}$ (AU)[d]	2.778 ± 1.476	2.522 ± 1.598
$\log g$ [b]	4.3059	4.5364
[Fe/H][c]	$+0.195$	$+0.231$
Common parameters		
Inclination to LOS, i ($^\circ$)[c]	79.20 ± 0.04	
Arg. of periapsis, ω ($^\circ$)[c]	231.65 ± 0.08	
Long. of asc. node, Ω ($^\circ$)[c]	204.85 ± 0.08	
Period (yr)[bc]	79.91 ± 0.01	
Eccentricity[c]	0.5179 ± 0.0008	
Semi-major axis, $r_{\rm AB}$ (AU)[c]	23.684 ± 0.64	
Distance (pc)[b]	1.348 ± 0.035	
Age (yr)	$(4.85 \pm 0.50) \times 10^9$	

[a] Kervella et al. (2003); [b] Torres et al. (2010); [c] Pourbaix et al. (2002); [d] Holman & Wiegert (1999); [e] Thévenin et al. (2002).

coefficients computed by Holman & Wiegert (1999) with significant error bars.

This expression was first computed from simulations of the $\alpha\,\mathrm{Cen}$-system which makes it convient for us. However, significant error bars prompted us to verify the accuracy of this expression with our own simulations.

Using known properties of the system (see Table 3.1) and the given c_1 to c_6 constants we could find the critical semi-major axis for each star, denoted $r_{\rm crit}$ in Table 3.1, again roughly $3 - 4$ AU for each star.

Finally we also know from e.g. Wiegert & Holman (1997); Jaime et al. (2012) that any circumbinary orbits are stable outside $\gtrsim 70 - 75$ AU.

The size limits are most important for us here as they give us realistic temperature limits for any dust emission.

We also ran complementing simulations. These solved the restricted three-body problem, i.e. massless particles in motion around the two stars in 3 di-

mensions. The code is a Runge-Kutta 4 code written by me in C. The three disc possibilities, two circumstellar and one circumbinary, were simulated separetely and the stellar orbits were part of the simulation (as a small validity test).

Initial conditions were varied for the circumstellar and circumbinary runs. The circumstellar discs had 10^4 massless particles on initially circular orbits around the relevant star, and at most $5\,\mathrm{AU}$ from the star. The initial particle surface distribution was homogenous, and the thickness was varied. Different thickness settings were tested, e.g. no thickness, Gaussian distribution with a standard deviation of $0.5\,\mathrm{AU}$, or a flaring disc with thickness $0.1 \times R$. These simulations were in general run with a timestep of 0.01 yr for 10^3 binary periods, i.e. 8×10^4 yr. Longer runs were also made with e.g. 10^4 periods to test the stability.

The circumbinary runs had discs with outer radii of $100\,\mathrm{AU}$ and $200\,\mathrm{AU}$ and a Gaussian distributed thickness of 5 and $10\,\mathrm{AU}$ respectively. The particles were initially set on circular orbits around the stellar barycenter and they were distributed homogeneously. For these larger discs a time step of $0.1\,\mathrm{yr}$ was sufficient and the simulations were left running for 10^3 periods. Longer runs were tested with e.g. 2×10^4 yr.

Results from these runs can be seen in Figures 3.1 and 3.2. Here we see how accurate the previously cited limits are. The large error bars for the critical semi-major axes are because the expression could then be useful for more binaries than just $\alpha\,\mathrm{Cen}$.

Additional circumstellar disc simulations were done with even higher time step resolution but smaller radii. The reason for this was to fill the inner parts of the circumstellar discs with particles, the parts the previous simulations had too low resolution to be able to correctly simulate. These had an outer radius of just $1\,\mathrm{AU}$, a timestep of $10^{-4}\,\mathrm{yr}$ to reach inner radii of $0.03\,\mathrm{AU}$, and were only run for 10 binary periods. The final states of these discs could be combined with the larger circumstellar discs which instead have correctly simulated outer edges.

However, the discovery of the exoplanet $\alpha\,\mathrm{Cen\,B}$b (Dumusque et al. 2012) complicates the high resolution small disc around $\alpha\,\mathrm{Cen\,B}$. Initially this planet was disregarded due to its small mass which gives it a Hill radius of just $4 \times 10^{-4}\,\mathrm{AU}$. Our circum-$\alpha\,\mathrm{Cen\,B}$ disc first only reached in to $0.08\,\mathrm{AU}$ and the planet could be disregarded (as seen in the results of Paper II). The smaller,

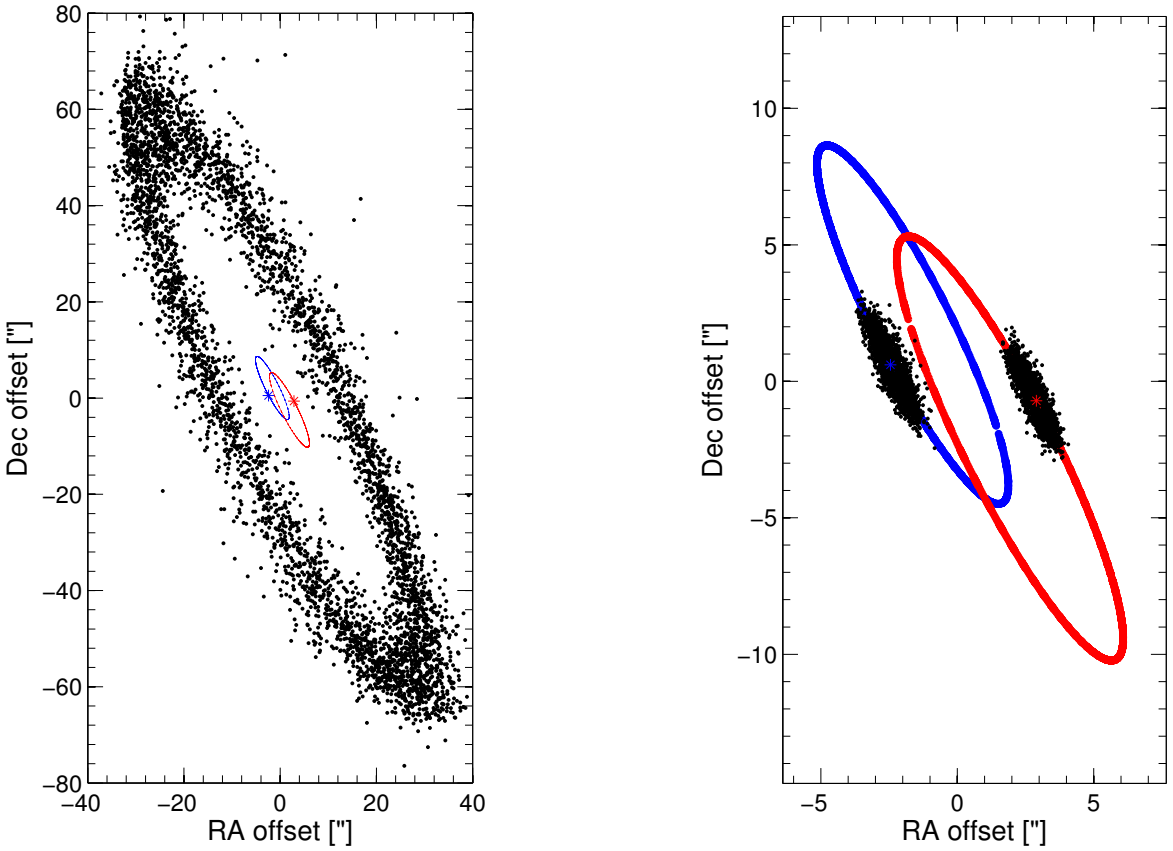

Figure 3.1: **Left:** circumbinary test particle disc in the stellar orbital plane as seen from the Earth. Outer radius is ~ 100 AU. **Right:** circumstellar test particle discs as seen from the Earth. Blue is α Cen A and its orbit, and red is α Cen B.

higher resolution disc however reaches all the way in to 0.03 AU while the semi-major axis of α Cen Bb is 0.04 AU.

In short: the combined, high-resolution discs were never used in Paper II, so there α Cen Bb was disregarded. In this thesis however, I also present results from the high-resolution discs. The existence of α Cen B is on the other hand questioned by Hatzes (2013), and is disregarded also in my high resolution simulations. If the planet does exist however, we can expect it to limit the amount of *hot* dust around 0.04 AU. Additional simulations involving the planet can be conducted if shown to be necessary.

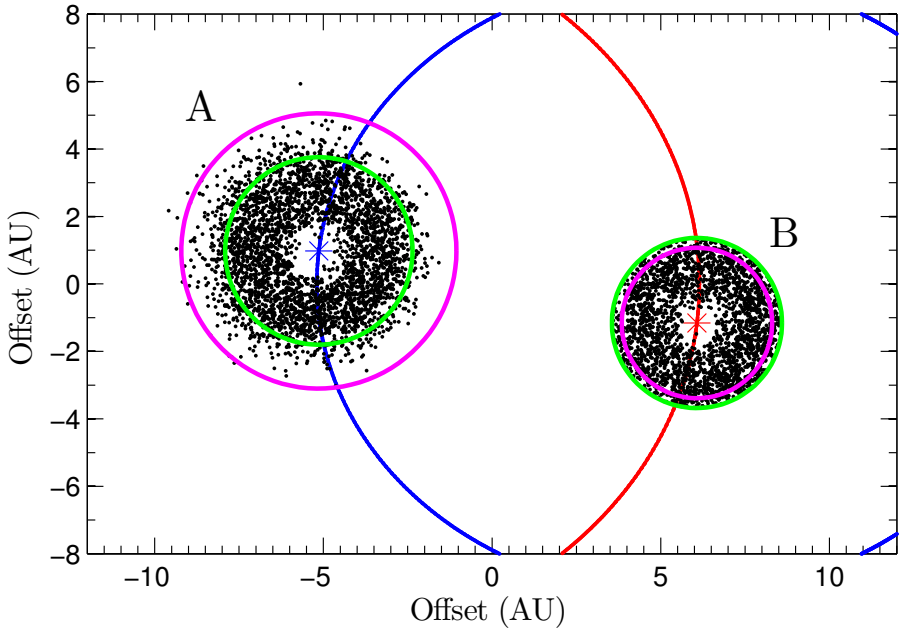

Figure 3.2: Circumstellar test particle discs for both stars, seen face on. The green circles correspond to the critical semi-major axis ($r_{\rm crit}$) and the purple circles correspond to the snow lines.

3.2 Observations

Through the DUNES Open Time Key Programme we obtained PACS photometric images at 100 μm and 160 μm. From the Hi-GAL survey we received archive PACS data at 70 μm and 160 μm and SPIRE data at 250, 350, and 500 μm. With APEX[1]-LABOCA (Large APEX BOlometer CAmera) we obtained data at 870 μm, and with SHeFI (Swedish Heterodyne Facility Instrument) APEX-1 we obtained complementing spectroscopic data to map CO emission in the region around α Cen. More details on these observations are presented in Paper II.

In Figure 3.3 we see the orbit of α Cen B around α Cen A and their positions during the observations. The two stars are currently approaching each other and will stay within 10″ on the sky during the coming 40 yr as seen from Earth. This will complicate future observations as they will not be resolved with anything except the largest telescopes. However, to observe them with these telescopes

[1] http://www.apex-telescope.org/telescope/

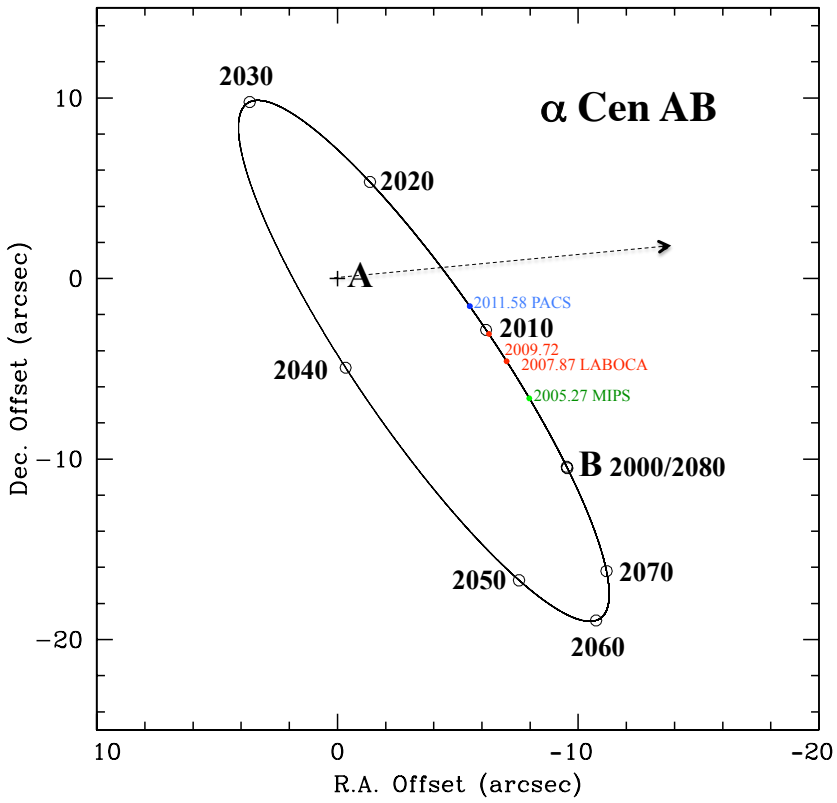

Figure 3.3: The orbit of $\alpha\,\mathrm{Cen\,B}$ around A as seen from the Earth. The coloured dates signify when the observations were done and the relative position of $\alpha\,\mathrm{Cen\,B}$ during these. The dashed arrow is the direction of the binary's proper motion, and the length of the arrow is the distance covered between the LABOCA (red, 2007-11-10 to 13) and PACS (blue, 2011-07-29) observations ($3\farcs7\,\mathrm{yr}^{-1}$). Green is the position of $\alpha\,\mathrm{Cen\,B}$ and the date of the MIPS observation (2005-04-09). $1''$ corresponds to $0.74\,\mathrm{AU}$ at this distance.

will instead bring us saturation problems as the stars are so luminous.

Because of the proximity of these stars they have a quite high proper motion of $3\farcs7\,\mathrm{yr}^{-1}$. The APEX-LABOCA and APEX-1 observations were made to be able to disentangle $\alpha\,\mathrm{Cen}$ and everything associated with these stars from the confusing background. These stars are on the southern hemisphere at declination $-61°$, in the direction of the galactic plane.

The observed flux densities of both stars are summarised in Table 3.2.

Table 3.2: Photometry and FIR/flux densities of α Centauri

$\lambda_{\rm eff}$ (μm)	α Cen A S_ν (Jy)	α Cen B S_ν (Jy)	Photometry & reference
0.440	2215 ± 41	536 ± 10	B (1)
0.550	3640 ± 67	1050 ± 19	V (1)
0.790	4814 ± 89	1654 ± 30	I (1)
0.440	2356 ± 43	572 ± 10	B (2)
0.550	3606 ± 66	1059 ± 20	V (2)
0.640	4259 ± 78	1387 ± 26	R_c (2)
0.790	4784 ± 88	1666 ± 31	I_c (2)
1.215	4658 ± 86	1645 ± 30	J (3)
1.654	3744 ± 69	1649 ± 31	H (3)
2.179	2561 ± 47	1139 ± 21	K (3)
3.547	1194 ± 22	521 ± 10	L (3)
4.769	592 ± 11	258 ± 5	M (3)
24	30.84 ± 0.76	13.63 ± 0.33	MIPS (4)
70	3.35 ± 0.28	1.49 ± 0.28	PACS (5)
100	1.41 ± 0.05	0.67 ± 0.037	PACS (6)
160	0.56 ± 0.06	0.21 ± 0.06	*PACS (5), (6)
250	0.24 ± 0.05	0.11 ± 0.05	*SPIRE (5)
350	0.145 ± 0.028	0.064 ± 0.028	*SPIRE (5)
500	0.08 ± 0.03	0.04 ± 0.03	*SPIRE (5)
870	0.028 ± 0.007	0.012 ± 0.007	*LABOCA (7)

* Asterisks indicate values determined using $S_{\nu,\,\rm A}/S_{\nu,\,\rm B} = 2.25$ see Paper I.

(1) HIPPARCOS, (2) Bessell (1990), (3) Engels et al. (1981).

(4) A. Mora [priv. com.; FWHM(24 μm) = 6″]. Binary separation on 9 April 2005, 10.″4

(5) Hi-GAL: KPOT_smolinar_1, fields 314_0 & 316_0. *Herschel*-beams FWHM(70 μm) = 5.″6, (100 μm) = 6.″8, (160 μm) = 11.″3, (250 μm) = 17.″6, (350 μm) = 23.″9, (500 μm) = 35.″2. Binary separation on 21 August 2010, 6.″3.

(6) DUNES: KPOT_ceiroa_1. Binary separation 29 July 2011, 5.″7.

(7) 384.C-1025, 380.C-3044(A): FWHM(870 μm) = 19.″5. Binary separation 20-13 November 2007, 8.″8 and 19 September 2009, 7.″0.

3.3 The SEDs of α Centauri

The observed fluxes (Table 3.2) are plotted in Figures 3.4 and 3.5. The stellar models plotted here were computed by a 3D interpolation in a smoothed version of the PHOENIX/GAIA grid (Brott & Hauschildt 2005). It used effective temperature and surface gravity from Torres et al. (2010) and metallicity from Thévenin et al. (2002), see Table 3.1.

These models span the wavelength region up to 45 μm, at longer wavelengths a black body extrapolation is assumed. The accuracy of this is discussed in Section 3.3.1.

In the SEDs we see marginal excesses at $24\,\mu$m of 2.5 and $2.6\,\sigma$ for $\alpha\,\mathrm{Cen\,A}$ and B respectively. These should correspond well to Zodiacal cloud dust temperatures and are studied in detail in Section 3.3.2.

We also see a flux dip at, and around, $160\,\mu$m. In the solar atmosphere, specifically at the lowest parts of the chromosphere, a few hundred kilometers above the photosphere, the Sun exhibits a temperature minimum (temperature less than T_{eff}). Above this the temperature rises again through the chromosphere and then the corona. The physics are however, not well understood.

In Paper I observations of this phenomenom in $\alpha\,\mathrm{Cen\,A}$ are discussed in detail. In Paper II we are more concerned with the effects on dust observations. The temperature inversion is probably common in solar-like stars, as visible in the histogram of Figure 6 of Eiroa et al. (2013).

In cases other than $\alpha\,\mathrm{Cen}$, where the observed fluxes coincide well with a stellar black body extrapolation, we risk missing small amounts of cold Kuiper belt analogue dust if a stellar temperature minimum is not considered. In Section 3.3.1 we use $\alpha\,\mathrm{Cen\,A}$ as a template for other, more distant stars, to discuss how much dust we risk missing.

Finally, we do not expect to see any excess from possible circumbinary dust in the SED. This is because the circumbinary dust is expected to exist at radii larger than 75 AU, well outside our beam size (if the disc is not seen edge-on).

3.3.1 Temperature minimum

In the lowest parts of the solar chromosphere the temperature drops below the effective temperature (around ~ 500 km above the photosphere, see e.g. Figure 4

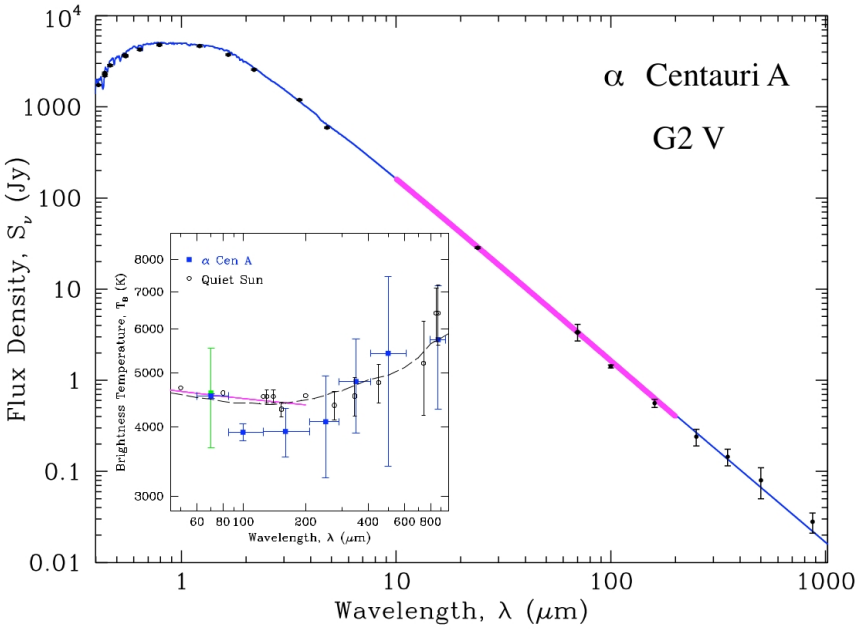

Figure 3.4: SED of α Cen A. Blue line is from a PHOENIX/GAIA model, the thick purple line is from an Uppsala model (up to 200 μm). Data points are presented in Table 3.2. The inset figure shows the FIR brightness temperature of α Cen A (blue squares) and of the Sun (black circles, Gu et al. 1997; Loukitcheva et al. 2004). Dashed black curve is from a semi-empirical chromosphere model for the Sun (Vernazza et al. 1981). See Paper I for details.

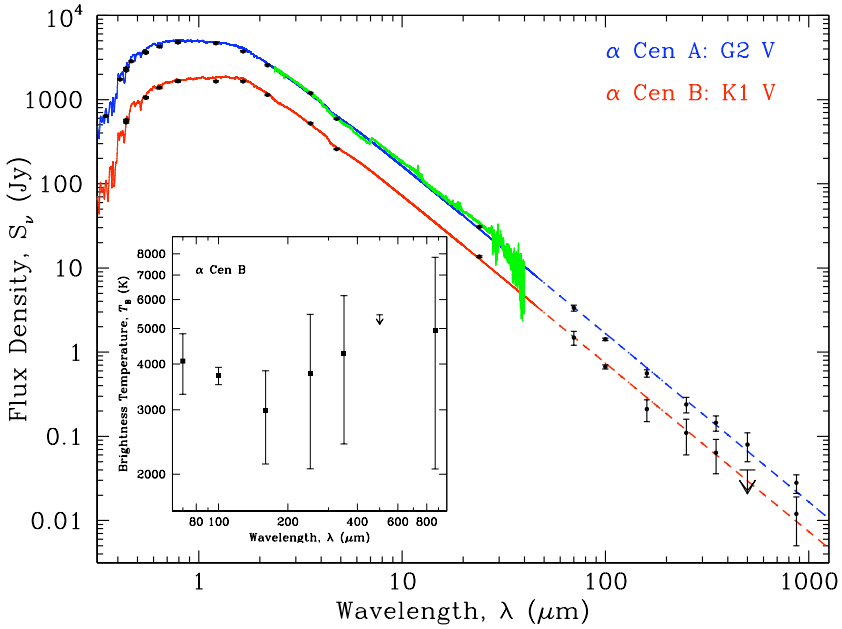

Figure 3.5: SEDs of α Cen. Same as in Figure 3.4 for α Cen A, red line is from a PHOENIX/GAIA model for α Cen B. Dashed lines correspond to where black body extrapolations are assumed. Data points are from the observed flux densities in Table 3.2. Green is an ISO-SWS low resolution observation (see Decin et al. 2003). The inset figure shows the FIR brightness temperature of α Cen B.

of Avrett 2003). In the Sun this phenomenon is visible at wavelengths around $150\,\mu$m. In Paper I we present for the first time a similar detection in the FIR spectrum of $\alpha\,\mathrm{Cen\,A}$. In Paper II we also see (tentatively) a similar effect in the SED of $\alpha\,\mathrm{Cen\,B}$, see Figure 3.5.

This is expected to be common in other solar-like stars, and to be visible in the $100-200\,\mu$m wavelength region because H^- free-free interactions limits the visibility of the photosphere at these wavelengths. These, and other observations (see Eiroa et al. 2013) are the first steps to help understanding the underlying physics.

In the case of $\alpha\,\mathrm{Cen\,A}$ we found a minimum temperature of $T_{\mathrm{min}} = 3920 \pm 375\,\mathrm{K}$, and for $\alpha\,\mathrm{Cen\,B}$, $T_{\mathrm{min}} = 3020 \pm 850\,\mathrm{K}$ near $160\,\mu$m. It is common to express the temperature minimum as the ratio $T_{\mathrm{min}}/T_{\mathrm{eff}}$. In our case we find the temperature ratios $T_{\mathrm{min}}/T_{\mathrm{eff}} = 0.67 \pm 0.06$ for $\alpha\,\mathrm{Cen\,A}$, and $T_{\mathrm{min}}/T_{\mathrm{eff}} = 0.58 \pm 0.17$ for $\alpha\,\mathrm{Cen\,B}$. These are slightly lower than what has been observed in the Sun by Ayres et al. (1976), i.e. ~ 0.78, through optical observations of the Ca II K line. They also estimated the temperature minimum of $\alpha\,\mathrm{Cen}$ this way and found temperature ratios of 0.78 or 0.79 for $\alpha\,\mathrm{Cen\,A}$, and 0.71 or 0.72 for $\alpha\,\mathrm{Cen\,B}$ (depending on stellar properties).

$\alpha\,\mathrm{Cen}$ is a good "laboratory" for other solar-like stars. Because we do not expect to see any dust at these wavelengths, we can safely assume that we are observing the stars directly (more on circumbinary dust in Section 3.4). Thus we can use $\alpha\,\mathrm{Cen\,A}$ as a template for more distant stars that do have Kuiper belt dust. The question is how much dust emission is required to "fill" the temperature minimum so that the combined dust and stellar spectrum follows a stellar black body. This is the focus of Section 4.3 of Paper II.

In Figure 3.6 (bottom frame) we see the flux difference of the observation and extrapolation, $\Delta S = S_{\mathrm{model}} - S_{\mathrm{min}}$, of $\alpha\,\mathrm{Cen\,A}$ set at a distance of 10 pc (S_{min} is the observed flux density of the temperature minimum). To this curve we fitted modified black bodies, i.e. dust emission models written as

$$S_{\mathrm{dust}} \approx B_\nu(T_{\mathrm{dust}}) \left(\frac{\nu}{\nu_0}\right)^\beta \times \mathcal{D} \tag{3.2}$$

where T_{dust} is set to correspond with the peak wavelength of ΔS (isothermal dust is assumed). This gives a dust temperature of $53\,\mathrm{K}$. $\mathcal{D}$ serves as a dilution

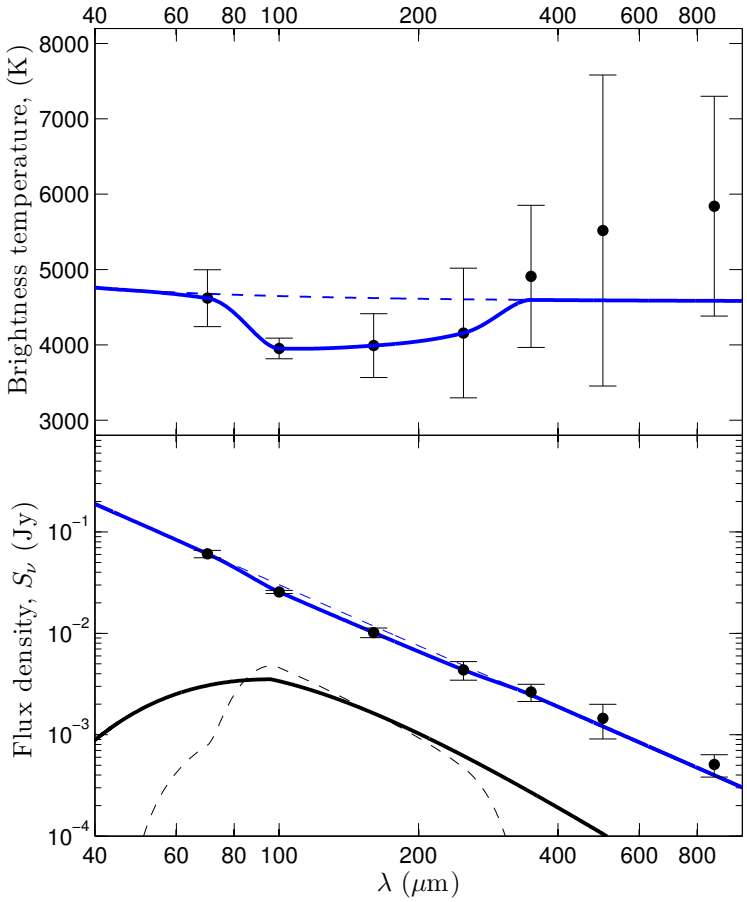

Figure 3.6: The part of the FIR spectrum of $\alpha\,\mathrm{Cen\ A}$ (blue) with the temperature minimum. The dashed blue line corresponds to the black body extrapolation of the stellar spectrum model. **Top:** the flux density of $\alpha\,\mathrm{Cen\ A}$ is expressed as brightness temperature. **Bottom:** the flux density with $\alpha\,\mathrm{Cen\ A}$ moved to a distance of $10\,\mathrm{pc}$. The dashed black line corresponds to ΔS, the difference in model flux and observation, and the thick black line corresponds to a dust black body with the temperature $53\,\mathrm{K}$.

factor (compare with Equation 2.11), and β was varied.

It is common to express the strength of dust emission as a fractional luminosity, $f_d \equiv L_{\rm dust}/L_\star$. So with $\alpha\,{\rm Cen\,A}$ as a template, we can deduce that the difference in flux corresponds to emission with a fractional luminosity, $f_d = \left(2.2\,^{+1.2}_{-1.5}\right) \times 10^{-7}$. This is comparable with the system Kuiper belt debris with a fractional luminosity of $\sim 10^{-7}$ (Vitense et al. 2012).

A fractional luminosity of 10^{-7} is however very small and difficult to detect. The *Herschel* space observatory for example, is estimated to have been able to observe Kuiper belts with a fractional luminosity of $\gtrsim 10^{-6}$ (Eiroa et al. 2013).

It is also possible to estimate, to the first order, a corresponding total dust mass from ΔS. Using the Hildebrand (1983) mass estimate (Equation 2.12) we can exchange the dust flux density $S_{\rm dust}$ with $\Delta S = S_{\rm model} - S_{\rm min}$. The mass absorption coefficient, $\kappa_{\rm abs}$ depends on e.g. dust grain size distribution and grain size limits. By studying the literature we can assume a value of $\gtrsim 10\,{\rm cm^2\,g^{-1}}$ (with particles smaller than $1\,{\rm mm}$ and a size distribution $\propto a^{-3.5}$) for this estimate (see e.g. Miyake & Nakagawa 1993; Ossenkopf & Henning 1994; Draine 2006, and references therein).

Using these assumptions, the observed flux density, black body extrapolation flux density, and the corresponding dust temperature of $53\,{\rm K}$, we find that the flux density difference can correspond to masses $\lesssim 10^{-3}\,M_{\rm Moon}$.

3.3.2 Circumstellar dust

From studies of the dynamics, we already know to what extent stable circumstellar orbits are possible around each of the two stars. Because these stable regions are smaller than $3-4\,{\rm AU}$, it is difficult not to be reminded of the solar system asteroid belt and Zodiacal dust cloud.

From the *Spitzer* observations presented in Paper II and Figure 3.5 we can deduce tentative excesses at $24\,\mu{\rm m}$ for both $\alpha\,{\rm Cen\,A}$ and B of just 2.5 and $2.6\,\sigma$. If interpreted as dust emission this corresponds to dust in the circumstellar regions. We aim here to model discs in these stable regions, and to set upper limits on fractional luminosities and mass estimates.

To correcly model these discs we chose to use a radiative transfer program called RADMC–3D by Dullemond (2012)[2]. This is a Monte-Carlo based radia-

[2] http://www.ita.uni-heidelberg.de/~dullemond/software/radmc-3d/

tive transfer program in the FIR for a dusty medium in 3 dimensions and is well suited for our needs.

This program does not include any previous assumptions on dust grain properties, dust masses, or disc shape. To run the program we need to include; (i) stellar spectra and positions, (ii) a 3D grid of dust mass densities, i.e. total dust mass is here one of the input parameters, and (iii) dust opacity properties, i.e. mass absorption and mass scattering coefficients, $\kappa_{\rm abs}$ and $\kappa_{\rm scat}$.

The stellar spectra and positions we already have. The spectra were computed through an adapted PHOENIX/GAIA grid (Brott & Hauschildt 2005), and the positions corresponding to the PACS $160\,\mu$m observations were used.

As for the grid of mass densities we already have simulated test particle discs. By assuming a total dust mass, radial power law density distribution, and homogenous radial particle size distribution (in fact by approximating the dust dynamics to the simplest model) we obtain a 3D distribution of masses with a "soft" outer edge based on the binary dynamics. The radial density distribution was adapted to the form $\Sigma = \Sigma_0\,(R/R_0)^{-\gamma}$. The final step was just to insert a grid and find how much mass is in each grid cube, which directly gives us total mass density of each grid coordinate.

In the mass absorption coefficient the grain size limits, grain size distribution, and grain mass density are included, i.e. $\kappa_{\rm abs}(a_{\rm min}, a_{\rm max}, q, \rho)$, where q is from the grain size distribution (see Chapter 2) written as $n(a_n) \propto a^{-q}$ (Dohnanyi 1969). We assume here that the grains sizes are homogenously distributed in the disc, without regard to their sizes.

In the literature it is easy to find several references with absorption coefficients. We turned to the work by Miyake & Nakagawa (1993) who computed the coefficients for spherical grains of different sizes, size ranges, and grain size distributions.

To summarise the grain properties used for the absorption: the blow-out radius of grains around $\alpha\,\mathrm{Cen\,A}$ (mass density of $2.5\,\mathrm{g\,cm^{-3}}$) is 0.64 μm. We can approximate the minimum grain size to be six times as large (see Chapter 2), i.e. $\sim 4\,\mu$m. Furthermore, the observed emission is at a wavelength of $24\,\mu$m. We can thus infer that the minimum grain size, which also dominates the emission we are observing, are also $\sim 4\,\mu$m. This is usually assumed to be roughly $\lambda/(2\,\pi)$. We also know from Miyake & Nakagawa (1993) that larger grains ex-

hibit less, or none, resonances. Largest grain size is as usual limited to $1\,\mathrm{mm}$. Miyake & Nakagawa (1993) also computed absorption coefficients with size distributions with $q = 2$, 2.5, 3, 3.5, and 4.

The albedo is trickier. Miyake & Nakagawa (1993) assume ice covered grains in their computations of the albedo, with the result of very high albedo in the optical. However, by computing the radii of the snow lines around both stars (see Section 2.2) we found that ice-covered grains seem unlikely in the stable regions (see more details in Paper II and Figure 3.2 where the ice lines are plotted). From Inoue et al. (2008) we learn that the albedo is roughly half of ice-free silicates for $\sim 10\,\mu\mathrm{m}$ grains, which gives us more realistic albedo models. Finally we assume isotropic scattering, which is the default setting in RADMC–3D.

Summary of the resulting SED models

I here now present results from more high resolution discs that stretches from $0.03\,\mathrm{AU}$ (the grain evaporation temperature is $\sim 1500\,\mathrm{K}$ and corresponds to roughly $0.03\,\mathrm{AU}$ from the stars) out to the critical semi-major axis. These discs have radial surface density distributions formulated as $\Sigma(R) = \Sigma_0\,(R/R_0)^{\gamma}$, with γ varying from 0 to a maximum of 10. $\gamma > 2$ represent small rings close to the star.

Figures 3.7 and 3.8 shows dust SEDs for both $\alpha\,\mathrm{Cen\,A}$ and B as computed with RADMC–3D. The discs here have $\gamma = 0$, and the different frames are for different q. To set upper limits the dust emission was constrained by the observations at 5, 24, and $70\,\mu\mathrm{m}$, where the observed fluxes at $70\,\mu\mathrm{m}$ correspond well with the stellar models. One SED of each plot matches the $24\,\mu\mathrm{m}$ flux. However, none of these fits within the error at $70\,\mu\mathrm{m}$. This tells us that the dust distribution must be either more radially constrained or that the emission must be weaker.

The $\alpha\,\mathrm{Cen\,B}$ observations have larger errors in general than the $\alpha\,\mathrm{Cen\,A}$ observations and were easier to fit emissions to. These observations allow discs with $\gamma \gtrsim 1.0$. In Figure 3.9 one model SED is shown for $\alpha\,\mathrm{Cen\,B}$ with $\gamma = 1.0$ and $q = 3.5$. For $\alpha\,\mathrm{Cen\,A}$ only extremely constrained rings close to the star ($\gamma > 6.0$ for example) would give model fluxes that are inside the $70\,\mu\mathrm{m}$ error.

However, for $\alpha\,\mathrm{Cen\,A}$ acceptable models tend to have a fractional luminosities of roughly $f_{\mathrm{d}} < 2 \times 10^{-5}$. For $\alpha\,\mathrm{Cen\,B}$ similar models have fractional

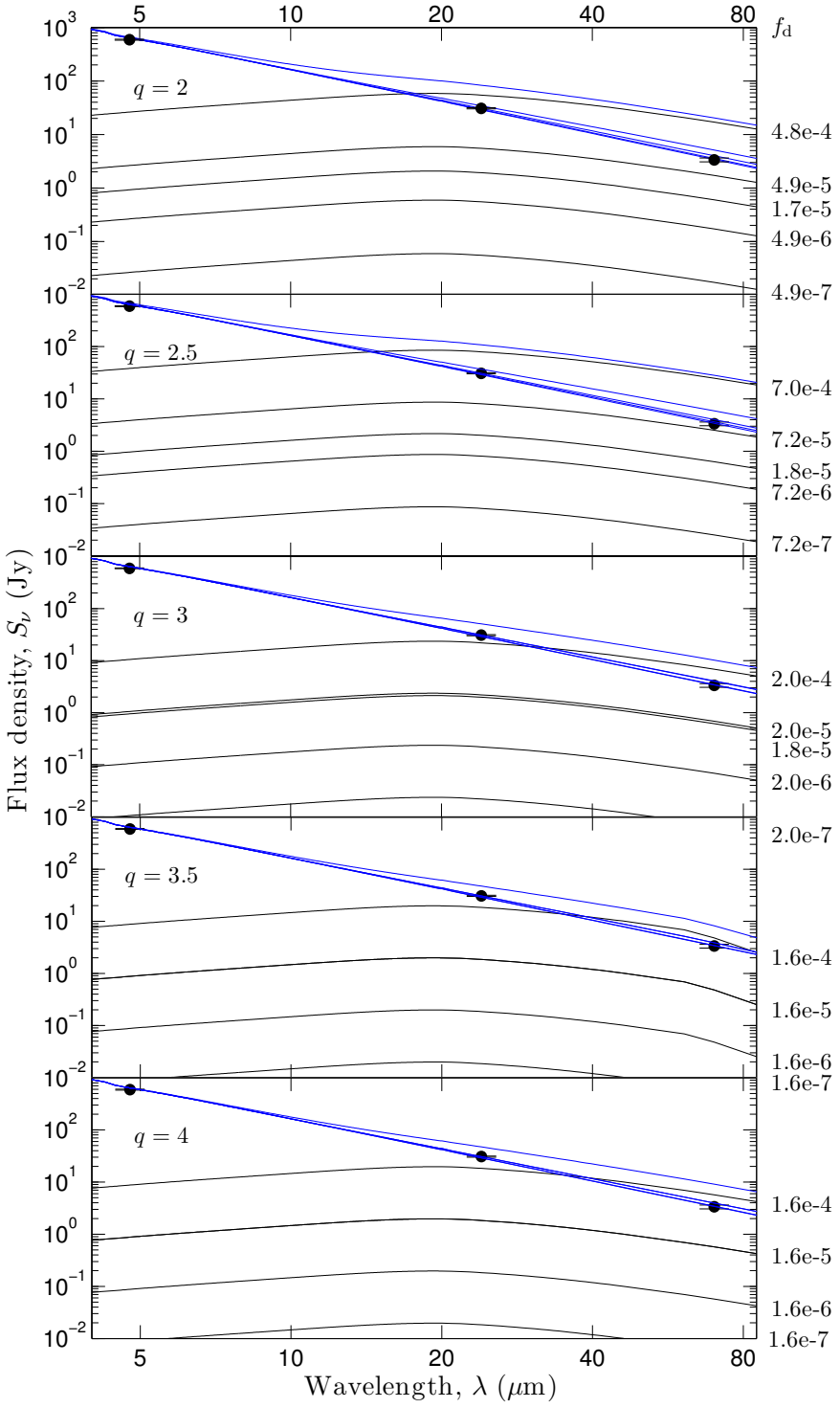

Figure 3.7: Dust emission models for α Cen A with circumstellar dust discs with various grain size distributions (varying q) and flat radial disc density distribution ($\gamma = 0$). Black lines are dust emission (corresponding fractional luminosities to the right) and blue lines are combined dust and stellar emission.

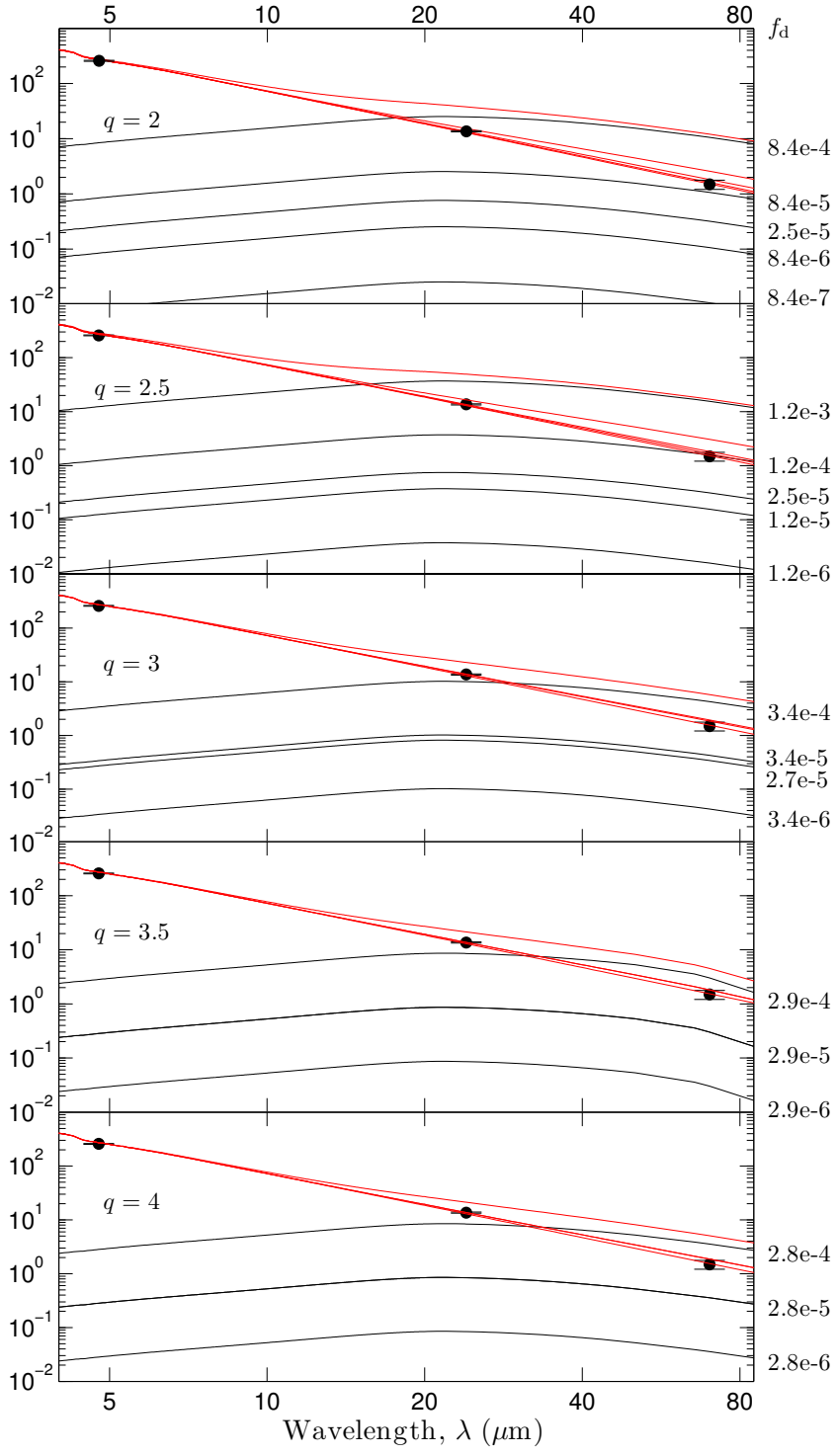

Figure 3.8: Dust emission models for α Cen B with circumstellar dust discs with various grain size distributions (varying q) and flat radial disc density distribution ($\gamma = 0$). Black lines are dust emission (corresponding fractional luminosities to the right) and red lines are combined dust and stellar emission.

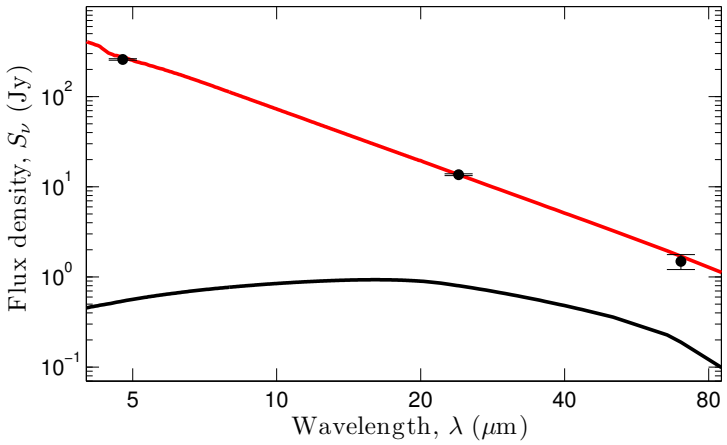

Figure 3.9: α Cen B SED with dust emission (black curve) from a dust disc with $\gamma = 1.0$, $q = 3.5$. Red curve is the combined stellar and dust spectrum.

luminosities of $f_\mathrm{d} < 3 \times 10^{-5}$. More radially constrained discs, i.e. with $\gamma \sim 1$ around α Cen B are warmer and have fractional luminosities of $f_\mathrm{d} < 4 \times 10^{-5}$. These results are in principal the same as published in Paper II.

These models correspond to total dust masses (grain sizes between $4\,\mu$m and 1 mm) of roughly 10^{-5} to $5 \times 10^{-6}\,M_\mathrm{Moon}$ when assuming size distributions with $q = 3.5$. In general, the models with $q = 3.5$ or $q = 4$ fit the data better than corresponding discs with smaller q.

3.4 Circumbinary dust

Circumbinary orbits are allowed at radii $\gtrsim 75$ AU from the stellar barycenter. At a distance of 1.348 pc this corresponds to an angular size of $\sim 56''$, i.e. clearly resolvable at all PACS-wavelengths. In this section I summarise the discussion in Paper II concerning circumbinary dust.

What such a ring should look like depends on its inclination and outer radius. The Kuiper belt in the solar system, for example, is estimated to have an outer radius of some 55 AU (Vitense et al. 2012, and references therein). There are examples of much larger debris discs such as the Fomalhaut ring with an outer radius of some 200 AU (Acke et al. 2012, and references therein). The outer radius is unconstrained by the dynamics, so the outer radii of the simulated discs

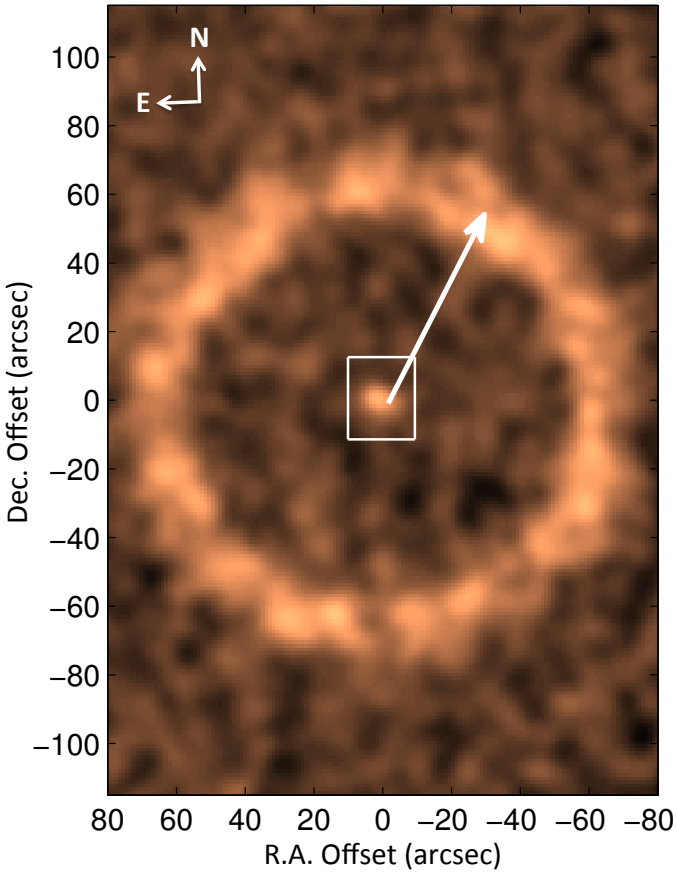

Figure 3.10: Synthetic observations of an face-on circumbinary ring around α Cen. The arrow represents a distance of 80 AU. The image was made with RADMC–3D with a disc with radius $\lesssim 100$ AU. Each pixel side is $1\farcs04$. The noise is Gaussian-distributed, and the image was smoothed with a Gaussian filter to mimic the beam size of the PACS-photometry (Figure 3.11).

we show here are purely due to initial conditions.

Figure 3.1 shows the results of particle simulations of a circumbinary ring with zero inclination to the binary orbital plane, and initial outer radius of 100 AU. The inclination can however, also be unconstrained for circumbinary rings (Wiegert & Holman 1997; Moutou et al. 2011), whereas circumstellar discs are limited to inclinations $< 60°$. Observations of the binary 99 Herculis for example, indicate that these stars have a circumpolar and circumbinary disc (Kennedy et al. 2012)

Figure 3.10 is a synthetic observation of a face-on ring, as seen from the Earth, around α Cen that represents what a circumbinary ring could look like at 160 μm. In the *Herschel*-PACS photometry shown in Figure 3.11 we do indeed see per-

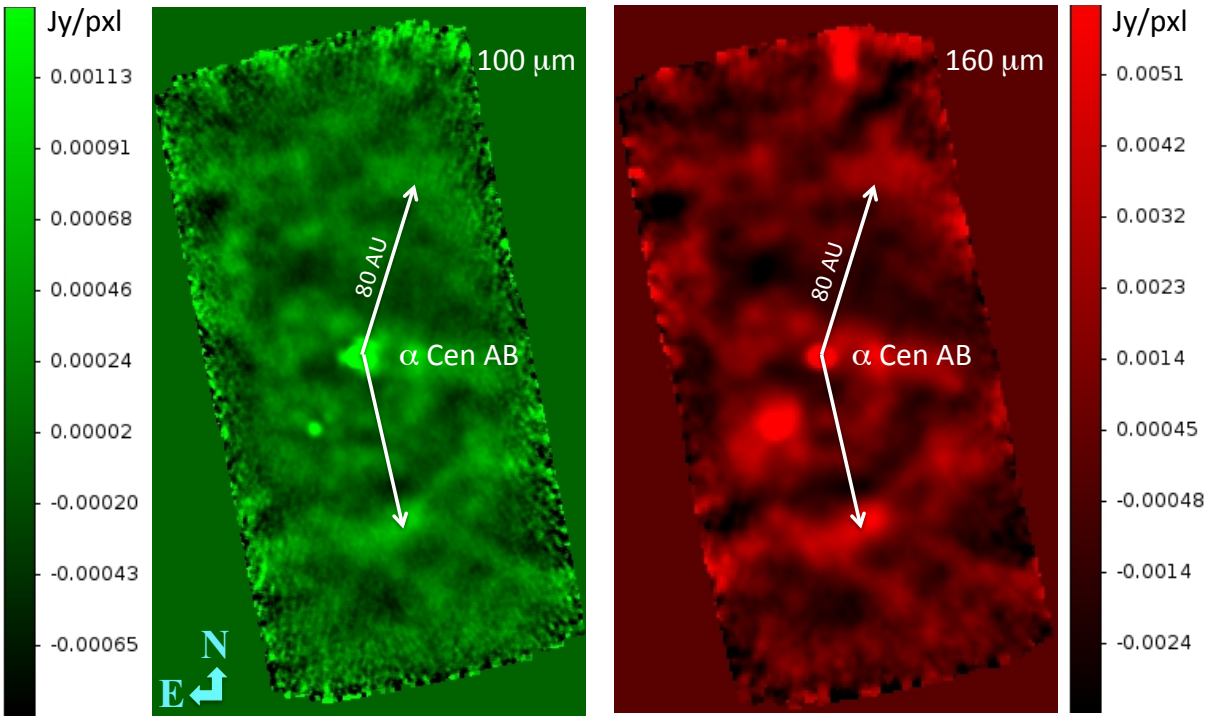

Figure 3.11: **Left:** *Herschel*–PACS photometry at 100 μmwith α Cen in the center and the arrows represent a distance of 80 AU from the stars, i.e. where circumbinary dust could be expected. **Right:** same as the left frame but with *Herschel*–PACS photometry at 160 μm.

sistent, curved/circular like structures at the correct angular distances from the stars.

To investigate if these structures are associated with α Cen, or the galactic background, CO $(2-1)$ was mapped with APEX, see Figure 3.12. We see here that both proper motion and spectral line data rule out that we have observed any circumbinary features associated with α Cen with *Herschel*. All detections have local-standard-of-rest (LSR) velocities of -30, -50, -60, and $40\,\mathrm{km\,s^{-1}}$ which agrees with observations of CO $(1-0)$ in the Milky Way (Dame et al. 2001). In conclusion; if there is any circumbinary dust associated with α Cen it remains undetected by us.

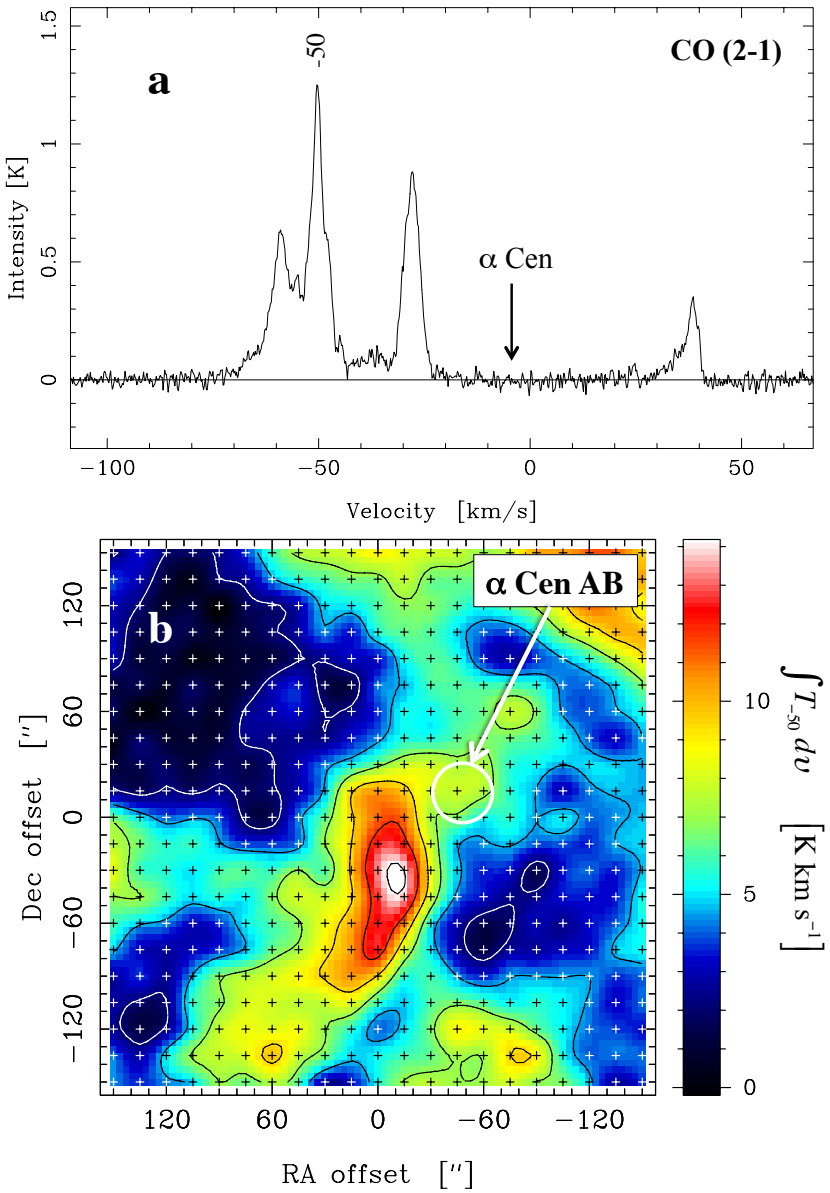

Figure 3.12: **a)** Average of all CO $(2-1)$ spectra toward α Cen plotted against $v_{\rm LSR}$. **b)** Map of the integrated CO $(2-1)$ line intensity in the region of α Cen at $v_{\rm LSR} = 50\,{\rm km\,s^{-1}}$. The center of the map is on the J2000 coordinates of α Cen B. The star was in the center of the white ring at the time of the observation (16 august 2012).

Chapter 4

Complex fields: a trio of stars

The ongoing project denoted *complex fields* (this name is a working title and might change in the future) involves three nearby stellar sources from the DUNES archive with distances up to 22 pc. The project working title refers to the fact that the sources are in fields containing much background confusion, a similar situation as with α Cen.

Herschel-PACS and SPIRE observations and first results on these stars are already published in the DUNES results paper by Eiroa et al. (2013). There also exist *Spitzer* data for all of these stars (Trilling et al. 2008).

In this project we have additional APEX-LABOCA observations at 870 μm. The idea is that by having multi-epoch observations we should be able to disentagle background sources from the stellar sources because of the proper motion of such nearby sources. Flux densities at longer wavelengths are of course also useful for constraining the Rayleigh-Jeans tail of circumstellar dust emission. However, preliminary results indicate that we only obtain upper limits at 870 μm on the total flux densities of the stars.

As this is an ongoing project, I only present background information found in the literature. Herschel data reduction and preliminary analysis are described by Eiroa et al. (2013).

4.1 HIP 4148

The first source, HIP 4148 (also HD 5133 and Gliese 42) was observed at all three PACS wavelengths (70, 100, and 160 μm). The star is a K2 V star with

Table 4.1: Properties and position of sources.

Source name	RA (J2000)	DEC (J2000)	Spectral class	Distance (pc)
HIP 4148	00h 53m 1.13s	-30° 21′ 24.″90	K2 V	12.22 ± 1.58
HIP 13402	02h 52m 32.13s	-12° 46′ 10.″97	K1 V	10.35 ± 0.04
HIP 14954	03h 12m 46.44s	-1° 11′ 45.″96	F8 V	22.6 ± 0.1

$^{(a)}$ Eiroa et al. (2013); $^{(b)}$ Trilling et al. (2008).

an effective temperature of 4940 K and a slightly lower metallicity [Fe/H] than the Sun of -0.15 (based on average values from a number of references, see Appendix B of Eiroa et al. 2013). Its age is cited at between 1.8 to 3.6 Gyr.

In the SED shown in Figure 4.1 we also see previous *Spitzer* MIPS observations up to $70\,\mu$m. The higher flux density found with MIPS $70\,\mu$m is due to background contamination (Eiroa et al. 2013). However, the higher resolution of *Herschel* remedies this and we can instead see the cold dust excess from the star.

Existing estimates indicate that this excess corresponds to circumstellar dust with black body temperature or 32 K at a radial distance of 41.2 AU from the star (Eiroa et al. 2013). The fractional luminosity of the excess is 9.4×10^{-6}.

We see a number of unknown background sources in the PACS images (Figure 4.2), with three of them clustered around the star in the image. These were not detected in the LABOCA images. One of them is listed in both Simbad[1] and NED[2] archives as the galaxy B005034.48-303540.9. Near the star, to the south west an X-ray source is also listed. No other background source was found in these archives.

4.2 HIP 13402

This star is one of the youngest in the DUNES sample with an age of $130 - 400$ Myr (it is also denoted as HD 17925, or EP Eri). It is a K1 V star and slightly colder than the Sun with an effective temperature of 5080 K, and it has a metallicity ([M/H]) of -0.15 (Trilling et al. 2008). The DUNES archive cites somewhat

[1]SIMBAD Astronomical Database: `http://simbad.u-strasbg.fr/simbad/`
[2]NASA/IPAC Extragalactic Database: `http://ned.ipac.caltech.edu/`

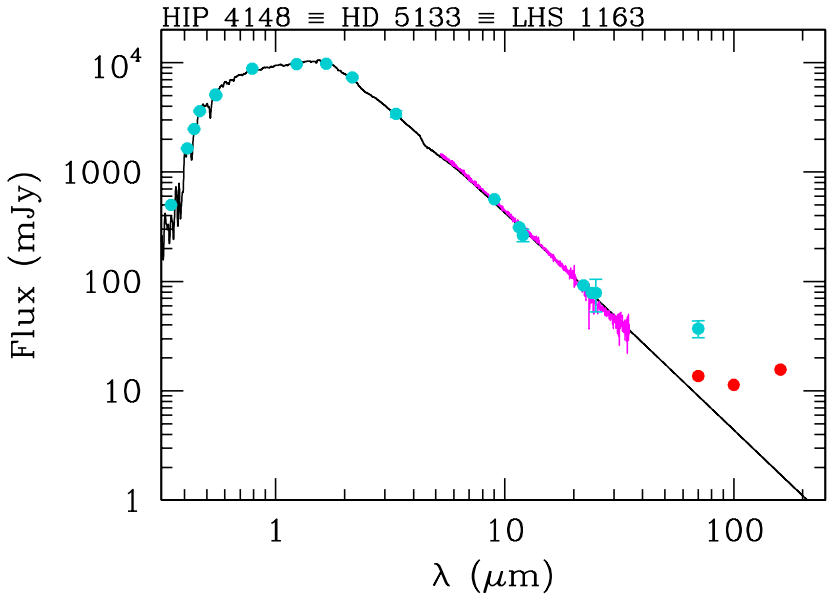

Figure 4.1: SED of HIP 4148, extracted from the DUNES data archive. Red points are from *Herschel*–PACS, cyan points at 24 and 70 μm are from *Spitzer* MIPS, and 12 and 25 μm points are from IRAS. The magenta spectrum is from *Spitzer* IRS. The black curve is from a PHOENIX/GAIA model.

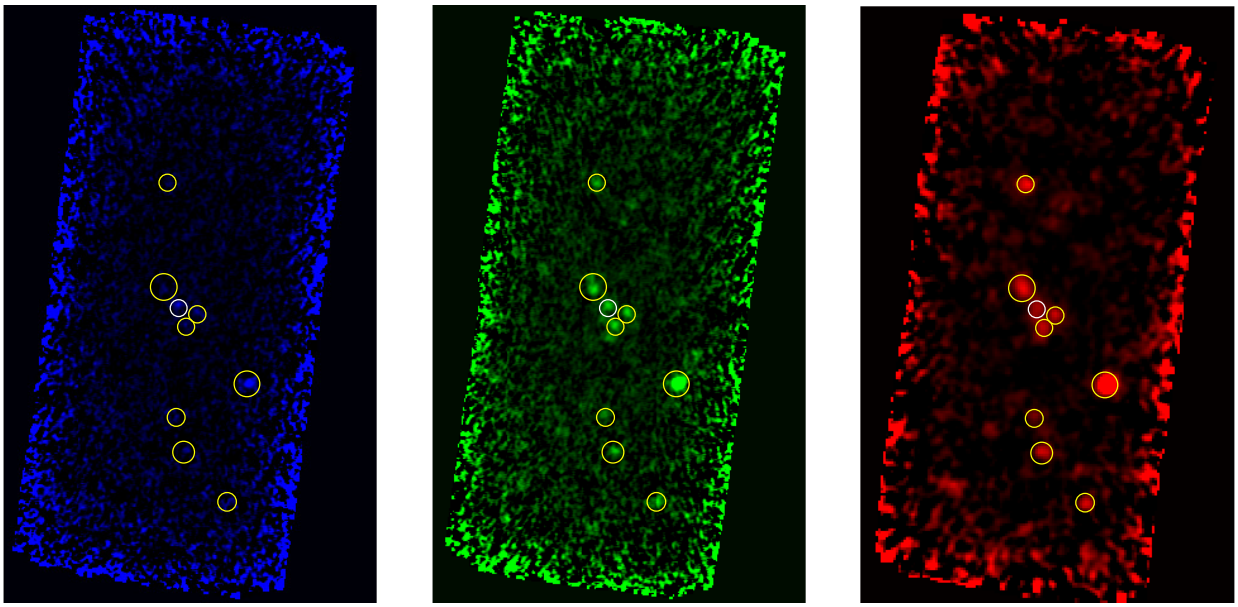

Figure 4.2: Herschel–PACS photometry of HIP 4148. Blue frame is 70 μm, green frame is 100 μm, and red frame is 160 μm. PACS images are $1\farcm75 \times 3\farcm5$, centred on the tabulated coordinates for the star, and up is north, left is east. The white ring is HIP 4148, yellow rings are possible background sources.

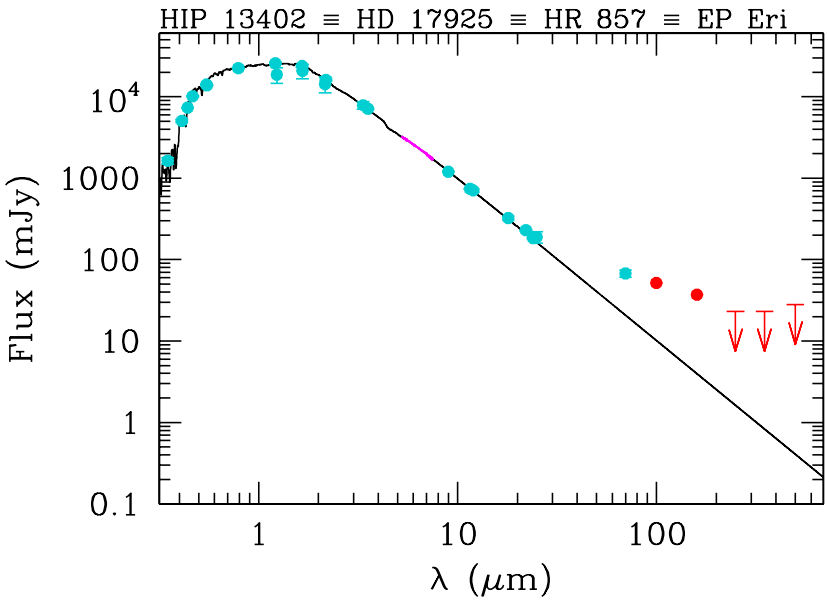

Figure 4.3: SED of HIP 13402, extracted from the DUNES data archive. Red points are from *Herschel*–PACS and red arrows are $3\,\sigma$ upper limits from SPIRE, cyan points at 24 and $70\,\mu$m are from *Spitzer* MIPS, and 12 and $25\,\mu$m points are from IRAS. The magenta spectrum is from *Spitzer* IRS. The black curve is from a PHOENIX/GAIA model.

more updated properties, i.e. $T_{\rm eff} = 5217$ K and the metallicity [Fe/H] of 0.1.

It has been speculated that this star might be an unresolved binary but Cutispoto et al. (2001) showed that this was not the case. However, it is probably a member of the Local Association (Maldonado et al. 2010).

The circumstellar dust was again first detected with *Spitzer* MIPS at $70\,\mu$m (Trilling et al. 2008, and references therein). It has since then also been observed with both *Herschel*-PACS and SPIRE at 100 to $500\,\mu$m (see Figure 4.3). Eiroa et al. (2013) give the dust excess a black body temperature of 52 K at a radial distance of 17.9 AU, and a fractional luminosity of 1.7×10^{-5}.

In the PACS $160\,\mu$m image there are 7 possible, unknown background sources that are not listed in Simbad or NED (see Figure 4.4). Five of these are visible also in the $100\,\mu$m image and one (maybe two) are visible in the $250\,\mu$m image.

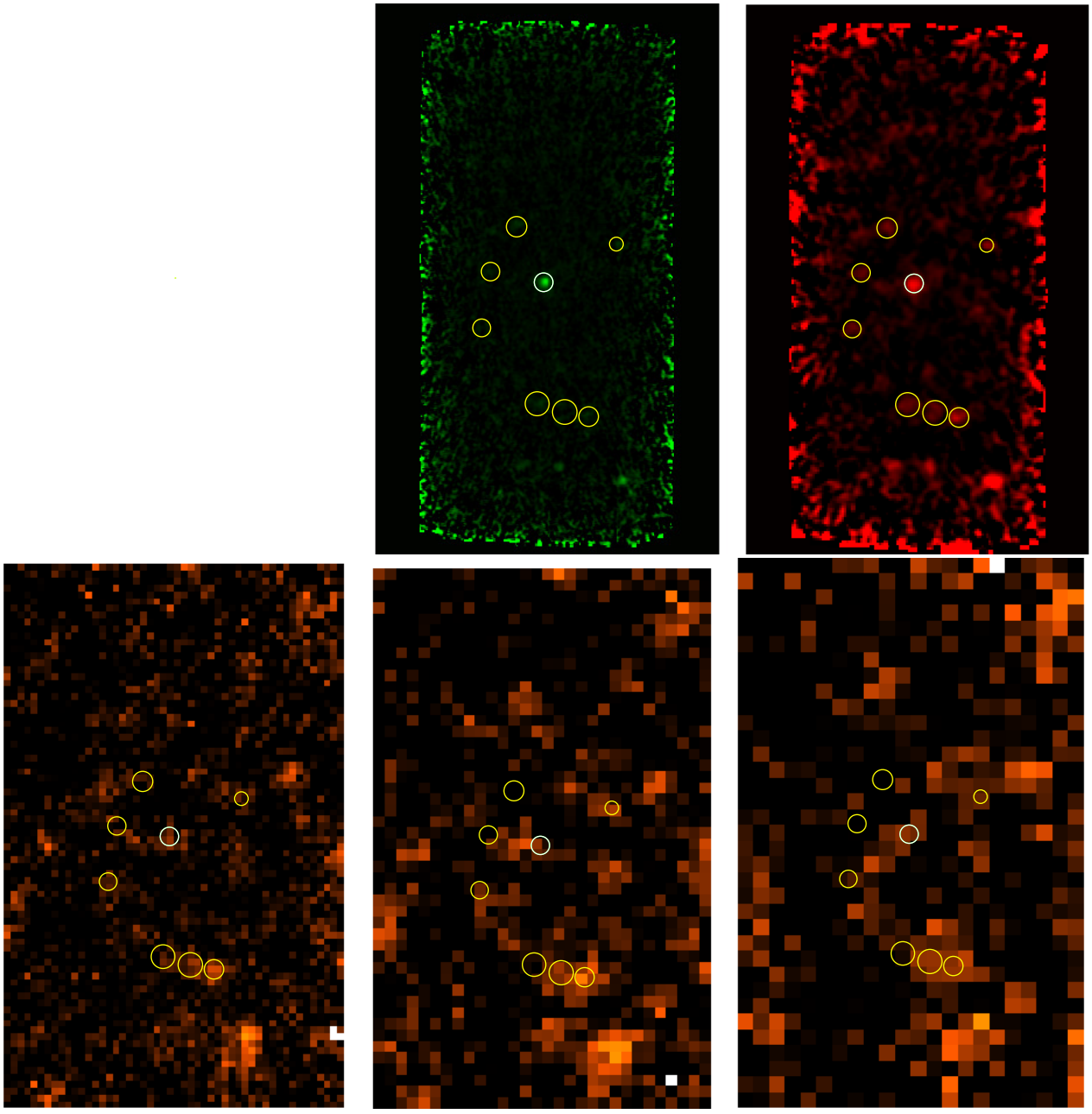

Figure 4.4: Herschel–PACS (top row) and SPIRE (bottom row) photometry of HIP 13802. Green frame is $100\,\mu$m, red frame is $160\,\mu$m, bottom frames are (from left to right) 250, 350, and $500\,\mu$m. PACS images are $1\farcm75 \times 3\farcm5$, the cut–out of the SPIRE images are $2\farcm5 \times 4'$, all are centred on the tabulated coordinates for the star, and up is north, left is east. The white ring is HIP 13402, yellow rings are possible background sources.

4.3 HIP 14954

This source, HIP 14954 (also known as HD 19994 and 94 Cet) is a binary. The primary star is an F8 V star with an effective temperature of 6187 K and metallicity ([Fe/H]) of 0.21 (Eiroa et al. 2013). The secondary is an M3 V star (Hale 1994) with a period of 2029 yr and semi-major axis of 220 AU (as found by Roberts et al. 2011 who recently refined the orbit and found a periapsis of 163 AU and the eccentricity 0.26). The angular, projected, separation is for the moment about $3\farcs3$, (Eiroa et al. 2013). At a distance of 22.6 pc the semi-major axis corresponds to an angle of roughly $9\farcs7$.

The primary star also has at least one associated planet, HIP 14954 b, detected in the CORALIE survey (Queloz et al. 2004; Mayor et al. 2004). It is estimated to have a semi-major axis of 1.4 AU, a period of 536 days, an eccentricity of 0.3, and the mass $m_{\rm b} \sin\, i = 1.7 M_{\rm Jup}$.

The dust emission was previously detected with *Spitzer* MIPS at $70\,\mu$m by Trilling et al. (2008). 100 and $160\,\mu$m photometry was then observed by DUNES (Eiroa et al. 2013) with Herschel-PACS (see Figure 4.6). A first estimate of the detected dust emission (see Figure 4.5) gives a black body temperature of 40 K which corresponds to a radial distance of 95.0 AU from the primary. The fractional luminosity is 4.2×10^{-5} (see Table 14 of Eiroa et al. 2013). This distance may coincide with the dynamically unstable region between the stars (Eiroa et al. 2013). Further dynamical studies are required to constrain the properties of this system.

We also see 5 unknown background sources in the PACS images. These show up in neither NED nor Sinbad archives. The positions and total fluxes of these will be mapped.

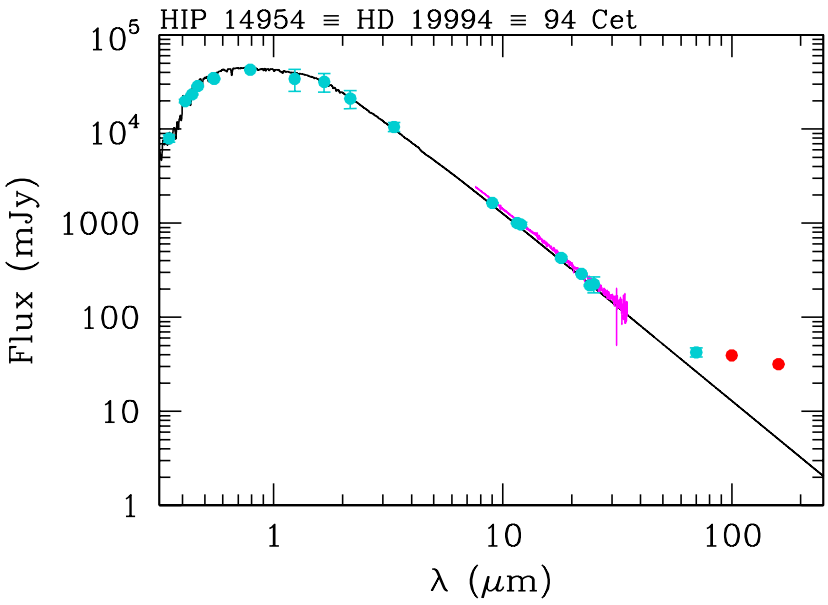

Figure 4.5: SED of HIP 14954, extracted from the DUNES data archive. Red points are from *Herschel*–PACS, cyan points at 24 and 70 μm are from *Spitzer* MIPS, and 12 and 25 μm points are from IRAS. The magenta spectrum is from *Spitzer* IRS. The black curve is from a PHOENIX/GAIA model.

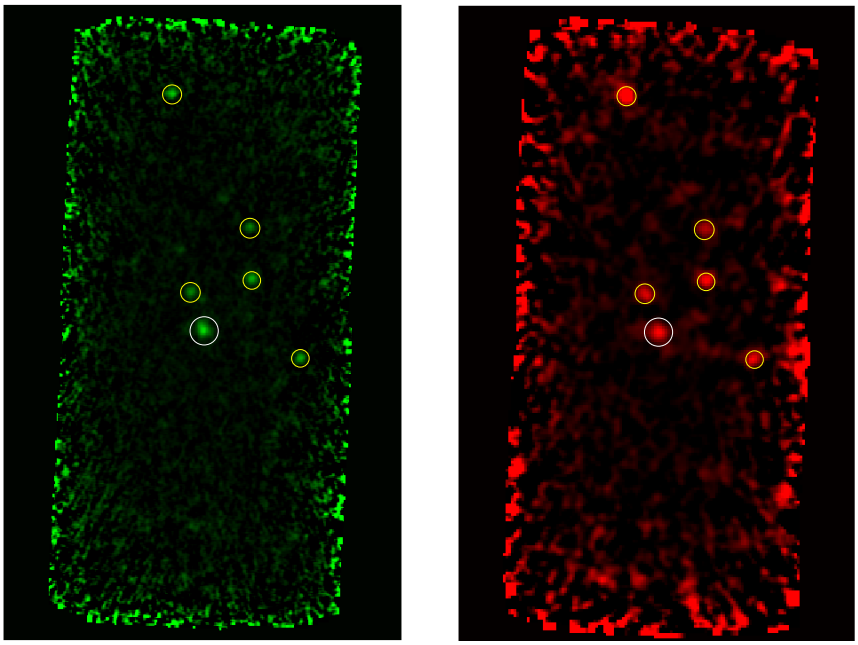

Figure 4.6: Herschel–PACS photometry of HIP 14954. Green frame is 100 μm and red frame is 160 μm. PACS images are $1\farcm75 \times 3\farcm5$, centred on the tabulated coordinates for the star, and up is north, left is east. The white ring is HIP 14954, yellow rings are possible background sources.

Chapter 5

Appended papers and future prospects

5.1 Summary of Paper I

This paper considers only the temperature minimum of $\alpha\,\mathrm{Cen\,A}$. Here we present the first detection of this phenomenom in another star than the Sun. This paper is included in this thesis due to the important implications it has for Paper II.

We find here that we have observed a chromospheric temperature minimum in $\alpha\,\mathrm{Cen\,A}$. This is estimated to a temperature of $T_{\mathrm{min}} = 3920 \pm 375\,\mathrm{K}$ and the ratio $T_{\mathrm{min}}/T_{\mathrm{eff}} = 0.67 \pm 0.06$.

5.2 Summary of Paper II

Most of the content of this paper is described in detail in Chapter 3. This paper covers two interesting issues. It discusses the possible amount of circumstellar and circumbinary dust at α Centauri, and it also discusses the implications of a solar-like temperature minimum (seen as a flux density dip when compared to a Rayleigh-Jeans tail in the stellar spectrum) would have on studies of Kuiper belt analogues of other, more distant stars.

We find tentative flux excesses of $\sim 2.5\,\sigma$ for both $\alpha\,\mathrm{Cen}$-stars, observed at $24\,\mu$m with *Spitzer*. If interpreted as dust emission we can set upper limits that correspond to fractional luminosity of $f_{\mathrm{d}} < 3 \times 10^{-5}$. As for the circumbinary possibility, we do not detect any dust emission.

As for the temperature minimum: we compute how much dust emission would be required to increase the observed flux density of $\alpha\,\mathrm{Cen\,A}$ to a black

body extrapolation at $160\,\mu$m. This would then be the amount of dust emission missed if a temperature minimum similar to that of $\alpha\,\mathrm{Cen\,A}$ is not considered when observing dust around other solar-like stars. In this case we find that this corresponds to emission with a fractional luminosity of $f_\mathrm{d} = \left(2.2\,^{+1.2}_{1.5}\right) \times 10^{-7}$.

5.3 Future prospects

In the near future I will continue the work on *Complex fields*. All the unknown background sources need to be mapped and more detailed dust modelling could be useful for all the stellar sources.

Of particular interest might HIP 14954 be, as this is a binary system. As stated by Eiroa et al. (2013) the dust here has been estimated to lie in the dynamically unstable region of the system and requires a more detailed analysis. A combination of dynamical and radiative transfer simulations, similar to what was done for $\alpha\,\mathrm{Cen}$, is probably what should be done here.

For the not so distant, and fairly distant future the outlooks are initially more unclear. Currently there are no available FIR space telescopes in operation after the shutdown of *Herschel*. Coming NASA budget cuts might also lead to the shutdown of SOFIA (Stratospheric Observatory for Infrared Astronomy, a $2.5\,$m telescope based on a Boeing 747, a joint project between NASA and the German aerospace center, Becklin 1997). And there are currently no new FIR space telescopes planned for the coming decade. However, there are ground based telescopes available today. The Atacama Large Millimeter/submillimeter Array (ALMA)[1] is probably most famous among these. ALMA does not, however, give the same possibilities as e.g. *Herschel* because it will not observe wavelengths shorter than $300\,\mu$m.

Ground based telescopes can obviously be maintained much more easily than space based telescopes. Also, interferometers have unrivaled angular resolution and are quite adaptable. However, the disadvantages are e.g. that FIR/submm wavelengths are extremely dependent on good, dry weather, which can vary even at the altitude of 5000 m of Llano de Chajnantor (the ALMA site). The competition for observation time at these new advanced telescopes is also high.

A really promising future, however, lies in exoplanet research. As mentioned

[1] `http://www.almaobservatory.org/`

before dust discs and planets are intricately coupled. A goal is to map out the contents of the nearest exoplanetary systems to understand the dynamics and evolution of them, and to put the solar system into context.

There are already several planet searching missions being planned e.g., PLATO (Planetary Transits and Oscillations of stars), CHEOPS (CHaracterising ExO-Planets Satellite), and TESS (Transiting Exoplanet Survey Satellite). Combining data with ground based telescopes (VLT and the coming E-ELT) will make it possible to map both the size and mass of exoplanets in the solar neighbourhood.

Bibliography

Acke, B., Min, M., Dominik, C., et al. 2012, A&A, 540, A125

Artymowicz, P. 1997, Annual Review of Earth and Planetary Sciences, 25, 175

Aumann, H. H. 1985, PASP, 97, 885

Aumann, H. H., Beichman, C. A., Gillett, F. C., et al. 1984, ApJL, 278, L23

Aumatell, G. & Wurm, G. 2011, MNRAS, 418, L1

Avrett, E. H. 2003, in Astronomical Society of the Pacific Conference Series, Vol. 286, Current Theoretical Models and Future High Resolution Solar Observations: Preparing for ATST, ed. A. A. Pevtsov & H. Uitenbroek, 419

Ayres, T. R., Linsky, J. L., Rodgers, A. W., & Kurucz, R. L. 1976, ApJ, 210, 199

Becklin, E. E. 1997, in ESA Special Publication, Vol. 401, The Far Infrared and Submillimetre Universe., ed. A. Wilson, 201–206

Bernstein, G. M., Trilling, D. E., Allen, R. L., et al. 2004, AJ, 128, 1364

Bessell, M. S. 1990, PASP, 102, 1181

Brott, I. & Hauschildt, P. H. 2005, in ESA Special Publication, Vol. 576, The Three-Dimensional Universe with Gaia, ed. C. Turon, K. S. O'Flaherty, & M. A. C. Perryman, 565

Campbell, B., Walker, G. A. H., & Yang, S. 1988, ApJ, 331, 902

Currie, T., Debes, J., Rodigas, T. J., et al. 2012, ApJL, 760, L32

Cutispoto, G., Messina, S., & Rodonò, M. 2001, A&A, 367, 910

Dame, T. M., Hartmann, D., & Thaddeus, P. 2001, ApJ, 547, 792

de Graauw, T., Helmich, F. P., Phillips, T. G., et al. 2010, A&A, 518, L6

Decin, L., Vandenbussche, B., Waelkens, K., et al. 2003, A&A, 400, 695

Dohnanyi, J. S. 1969, , 74, 2531

Draine, B. T. 1988, ApJ, 333, 848

Draine, B. T. 2003, ApJ, 598, 1017

Draine, B. T. 2006, ApJ, 636, 1114

Dullemond, C. P. 2012, RADMC-3D: A multi-purpose radiative transfer tool, astrophysics Source Code Library

Dumusque, X., Pepe, F., Lovis, C., et al. 2012, Nature, 491, 207

Eiroa, C., Marshall, J. P., Mora, A., et al. 2013, A&A, 555, A11

Endl, M., Kürster, M., Els, S., Hatzes, A. P., & Cochran, W. D. 2001, A&A, 374, 675

Engels, D., Sherwood, W. A., Wamsteker, W., & Schultz, G. V. 1981, , 45, 5

Ertel, S., Wolf, S., & Rodmann, J. 2012, A&A, 544, A61

Gáspár, A., Psaltis, D., Rieke, G. H., & Özel, F. 2012, ApJ, 754, 74

Gillett, F. C. 1986, in Astrophysics and Space Science Library, Vol. 124, Light on Dark Matter, ed. F. P. Israel, 61–69

Griffin, M. J., Abergel, A., Abreu, A., et al. 2010, A&A, 518, L3

Grigorieva, A., Thébault, P., Artymowicz, P., & Brandeker, A. 2007, A&A, 475, 755

Gu, Y., Jefferies, J. T., Lindsey, C., & Avrett, E. H. 1997, ApJ, 484, 960

Gustafson, B. A. S. 1994, Annual Review of Earth and Planetary Sciences, 22, 553

Hale, A. 1994, AJ, 107, 306

Hatzes, A. P. 2013, ApJ, 770, 133

Hatzes, A. P., Cochran, W. D., Endl, M., et al. 2003, ApJ, 599, 1383

Hatzes, A. P., Cochran, W. D., McArthur, B., et al. 2000, ApJL, 544, L145

Hildebrand, R. H. 1983, , 24, 267

Holman, M. J. & Wiegert, P. A. 1999, AJ, 117, 621

Inoue, A. K., Honda, M., Nakamoto, T., & Oka, A. 2008, , 60, 557

Jaime, L. G., Pichardo, B., & Aguilar, L. 2012, MNRAS, 427, 2723

Kalas, P., Graham, J. R., Chiang, E., et al. 2008, Science, 322, 1345

Kalas, P., Graham, J. R., Fitzgerald, M. P., & Clampin, M. 2013, ApJ, 775, 56

Kennedy, G. M., Wyatt, M. C., Sibthorpe, B., et al. 2012, MNRAS, 421, 2264

Kervella, P., Thévenin, F., Ségransan, D., et al. 2003, A&A, 404, 1087

Kral, Q., Thébault, P., & Charnoz, S. 2013, A&A, 558, A121

Krivov, A. V. 2010, Research in Astronomy and Astrophysics, 10, 383

Krivov, A. V., Eiroa, C., Löhne, T., et al. 2013, ApJ, 772, 32

Krivov, A. V., Löhne, T., & Sremčević, M. 2006, A&A, 455, 509

Krügel, E. & Siebenmorgen, R. 1994, A&A, 288, 929

Lagrange, A.-M., Gratadour, D., Chauvin, G., et al. 2009, A&A, 493, L21

Lamy, P. L. 1974, A&A, 35, 197

Liseau, R., Risacher, C., Brandeker, A., et al. 2008, A&A, 480, L47

Löhne, T., Augereau, J.-C., Ertel, S., et al. 2012, A&A, 537, A110

Löhne, T., Krivov, A. V., & Rodmann, J. 2008, ApJ, 673, 1123

Loukitcheva, M., Solanki, S. K., Carlsson, M., & Stein, R. F. 2004, A&A, 419, 747

Maldonado, J., Eiroa, C., Villaver, E., Montesinos, B., & Mora, A. 2012, A&A, 541, A40

Maldonado, J., Martínez-Arnáiz, R. M., Eiroa, C., Montes, D., & Montesinos, B. 2010, A&A, 521, A12

Marengo, M., Stapelfeldt, K., Werner, M. W., et al. 2009, ApJ, 700, 1647

Mathis, J. S., Rumpl, W., & Nordsieck, K. H. 1977, ApJ, 217, 425

Mayor, M. & Queloz, D. 1995, Nature, 378, 355

Mayor, M., Udry, S., Naef, D., et al. 2004, A&A, 415, 391

Miyake, K. & Nakagawa, Y. 1993, , 106, 20

Moro-Martin, A. 2013, Dusty Planetary Systems, ed. T. D. Oswalt, L. M. French, & P. Kalas, 431

Moutou, C., Díaz, R. F., Udry, S., et al. 2011, A&A, 533, A113

Ossenkopf, V. & Henning, T. 1994, A&A, 291, 943

Paardekooper, S.-J. & Leinhardt, Z. M. 2010, MNRAS, 403, L64

Pilbratt, G. L., Riedinger, J. R., Passvogel, T., et al. 2010, A&A, 518, L1

Plavchan, P., Werner, M. W., Chen, C. H., et al. 2009, ApJ, 698, 1068

Poglitsch, A., Waelkens, C., Geis, N., et al. 2010, A&A, 518, L2

Pollack, J. B., Hollenbach, D., Beckwith, S., et al. 1994, ApJ, 421, 615

Pourbaix, D., Nidever, D., McCarthy, C., et al. 2002, A&A, 386, 280

Queloz, D., Mayor, M., Naef, D., et al. 2004, in IAU Symposium, Vol. 202, Planetary Systems in the Universe, ed. A. Penny, 106

Regály, Z., Juhász, A., Sándor, Z., & Dullemond, C. P. 2012, MNRAS, 419, 1701

Roberts, Jr., L. C., Turner, N. H., ten Brummelaar, T. A., Mason, B. D., & Hartkopf, W. I. 2011, AJ, 142, 175

Roell, T., Neuhäuser, R., Seifahrt, A., & Mugrauer, M. 2012, A&A, 542, A92

Smith, B. A. & Terrile, R. J. 1984, Science, 226, 1421

Söderhjelm, S. 1999, A&A, 341, 121

Stark, C. C. & Kuchner, M. J. 2008, ApJ, 686, 637

Strubbe, L. E. & Chiang, E. I. 2006, ApJ, 648, 652

Thébault, P. 2012, A&A, 537, A65

Thébault, P. & Augereau, J.-C. 2007, A&A, 472, 169

Thébault, P., Marzari, F., & Augereau, J.-C. 2010, A&A, 524, A13

Thébault, P., Marzari, F., & Scholl, H. 2009, MNRAS, 393, L21

Thévenin, F., Provost, J., Morel, P., et al. 2002, A&A, 392, L9

Torres, G., Andersen, J., & Giménez, A. 2010, , 18, 67

Trilling, D. E., Bryden, G., Beichman, C. A., et al. 2008, ApJ, 674, 1086

Vernazza, J. E., Avrett, E. H., & Loeser, R. 1981, ApJS, 45, 635

Vitense, C., Krivov, A. V., Kobayashi, H., & Löhne, T. 2012, A&A, 540, A30

Wahhaj, Z., Koerner, D. W., Ressler, M. E., et al. 2003, ApJL, 584, L27

Walker, G. A. H., Bohlender, D. A., Walker, A. R., et al. 1992, ApJL, 396, L91

Wiegert, P. A. & Holman, M. J. 1997, AJ, 113, 1445

Wolszczan, A. & Frail, D. A. 1992, Nature, 355, 145

Wood, B. E., Linsky, J. L., Müller, H.-R., & Zank, G. P. 2001, ApJL, 547, L49

Wood, B. E., Müller, H.-R., Zank, G. P., Linsky, J. L., & Redfield, S. 2005, ApJL, 628, L143

Wyatt, M. C., Clarke, C. J., & Booth, M. 2011, Celestial Mechanics and Dynamical Astronomy, 111, 1

Xie, J.-W., Zhou, J.-L., & Ge, J. 2010, ApJ, 708, 1566

Zuckerman, B., Song, I., Bessell, M. S., & Webb, R. A. 2001, ApJL, 562, L87